LABPLAS

Horizon 2020
European Union Funding
for Research & Innovation

# Land-Based Solutions for Plastics in the Sea

*This project has received funding from the European Union's Horizon 2020 research and innovation programme under grant agreement No 101003954*

## D7.1 Technical report describing the ePLAS model

**Due date of deliverable: 31/01/2025**

**Actual submission date: 31/01/2025**

Horizon 2020
European Union Funding
for Research & Innovation

LABPLAS

Horizon 2020
European Union Funding
for Research & Innovation

## PROJECT INFORMATION

**Project number:** 101003954

**Project acronym:** LABPLAS

**Project full title:** Land-Based Solutions for Plastics in the Sea

**Call:** H2020-SC5-2018-2019-2020 submitted for H2020-SC5-2020-2 / 03 Sep 2020

**Topic:** CE-SC5-30-2020 – Plastics in the environment: understanding the sources, transport, distribution and impacts of plastics pollution

**Type of action:** RIA – Research and Innovation Action

**Starting date:** June 1st, 2021

**Duration:** 48 months

**List of participants:**

| Nº | Participant name | Acronym | Country | Type |
|---|---|---|---|---|
| 1 | UNIVERSIDADE DE VIGO | UVI | SPAIN | HES |
| 2 | UNIVERSIDADE DA CORUÑA | UDC | SPAIN | HES |
| 3 | Bundesanstalt fuer Gewaesserkunde | BfG | GERMANY | RTO |
| 4 | LABORATORIO IBERICO INTERNACIONAL DE NANOTECNOLOGIA | INL | PORTUGAL | RTO |
| 5 | KATHOLIEKE UNIVERSITEIT LEUVEN | KUL | BELGIUM | HES |
| 6 | HELMHOLTZ ZENTRUM FUR OZEANFORSCHUNG KIEL | GEOMAR | GERMANY | RTO |
| 7 | NATIONAL OCEANOGRAPHY CENTRE | NOC | UNITED KINGDOM | RTO |
| 8 | SORBONNE UNIVERSITE | SU | FRANCE | HES |
| 9 | OPEN UNIVERSITEIT NEDERLAND | OUNL | NETHERLANDS | HES |
| 10 | LEIBNIZ INSTITUTE FOR BALTIC SEA RESEARCH | IOW | GERMANY | RTO |
| 11 | ASSOCIACAO PARA O DESENVOLVIMENTO DO ATLANTIC INTERNATIONAL RESEARCH CENTRE | AC | PORTUGAL | RTO |
| 12 | UNIVERSIDADE FEDERAL DO SAO PAULO | UNIFESP | BRAZIL | HES |
| 13 | BASF SE | BASF | GERMANY | LE |
| 14 | TG ENVIRONMENTAL RESEARCH | ER | UNITED KINGDOM | SME |
| 15 | CONTACTICA S.L. | CTA | SPAIN | SME |
| 16 | STICHTING EGI | EGI | NETHERLANDS | Non-P |
| 17 | STICHTING RADBOUD UNIVERSITEIT | RU | NETHERLANDS | HES |
| 18 | UNIVERSIDADE FEDERAL DO PARÁ | UFPA | BRAZIL | HES |

## DELIVERABLE DETAILS

| | |
|---|---|
| **Document number:** | D7.1 |
| **Document title:** | Technical report describing the ePLAS model |
| **Dissemination level** | PU – Public |
| **Period:** | RP3 |
| **WP:** | WP7 |
| **Task:** | Task 7.1. |
| **Status:** | Final |
| **Author:** | Radboud University, Open Universiteit |
| **Reviewers:** | |
| **Recommended citation format** | Yichen, S., van Wijnen, J., Ragas, A.M.J., 2025, Technical report describing the ePLAS model, including case studies for the Elbe, Thames and Mero-Barcés river basins resulting from Task 7.1 activities applied to the case studies described in WP2, Deliverable 7.1, LABPLAS Grant Agreement No. 101003954 H2020-SC5-2020-2 |
| **Executive summary:** | This report describes the adaptation of the original process formulations of the ePiE model to enable the prediction and assessment of microplastic concentrations in European rivers, lakes and sediments. By utilizing the high spatial resolution (~1x1 km) and comprehensive data integration capabilities of the ePiE model, the updated model (ePLAS) aims to capture the complex transport dynamics of microplastics across extensive geographic areas, thus providing vital insights into their environmental dispersion and potential impacts. This adaptation not only extends the utility of the ePiE model but also enhances our capacity to address an emerging environmental challenge with significant ecological and health implications. |

| Version | Date | Comments |
|---|---|---|
| 1 | 2024 Oct 20 | First draft, reviewed by WP7 partners |
| 2 | 2025 Jan 29 | Final version |

**Disclaimer**

The views and opinions expressed in this document reflect only the authors' views, and not necessarily those of the European Commission.

## TABLE OF CONTENTS

PROJECT INFORMATION ..... 1
DELIVERABLE DETAILS ..... 2
TABLE OF CONTENTS ..... 3
ABBREVIATIONS AND ACRONYMS ..... 5
PREFACE ..... 6
1 INTRODUCTION ..... 7
2 MODELLING CONCEPT ..... 9
3 HYDROLOGY OF RIVERS AND LAKES ..... 11
4 EMISSION ESTIMATION ..... 15
4.1 Per capita emission ..... 15
4.2 European wastewater treatment plants and agglomerations ..... 15
4.3 Fate during wastewater treatment ..... 16
4.4 Allocation of emissions to river nodes ..... 0
4.4.1 Types of river nodes ..... 0
4.4.2 Point sources and diffuse sources ..... 0
5 CHARACTERIZATION OF MICROPLASTIC PARTICLES ..... 2
5.1 Tyre wear particles ..... 2
6 FATE PROCESSES ..... 7
6.1 Advection with water ..... 7
6.2 Sedimentation ..... 8
6.3 Resuspension ..... 8
6.4 Heteroaggregation ..... 10
6.5 Sediment transport ..... 12
6.6 Burial ..... 12
6.7 Bioturbation ..... 13
6.8 Mass balance equations ..... 13
6.8.1 Mass balance equation for free TWP particles (For Box = 1) ..... 14
6.8.2 Solving the mass balance equation under steady-state condition for the first box ..... 15
6.8.3 Solving the mass balance equation under steady state conditions for box = 2 to i ..... 16
LITERATURE ..... 19
SUPPLEMENTARY MATERIALS ..... 25

## LIST OF FIGURES AND TABLES

Figure 1. Fate processes of microplastics in the water layer, bed load layer and sediment layer……12

Figure 2. Applying the multimedia box model to river nodes schematic diagram……...12

Figure 3. Validation results of river discharge volume for year-specific annual mean (A), maximum (B), and minimum (C) monthly flow conditions. Independent validation dataset consisted of yearly measurements from 2010 to 2015 at 1,007 GRDC European stations. The solid line represents a perfect model fit (1:1 line), and the dashed lines indicate a difference of one order of magnitude……13

Figure 4. Schematic diagram of river nodes for different types (WWTP/Agglomeration will be added to the ePLAS model as a point source)……21

Figure 5. Particle size ranges and obtained TWP size distributions. 1 (Kwak et al., 2013); 2 (Dahl et al., 2006); 3 (Gustafsson et al., 2008); 4 (Kreider et al., 2010); 5 (Wang et al., 2017)……23

Figure 6. Particle size distribution of TRWP from Kreider et al. (2010) with lower and upper bounds of urban road and highway runoff distributions summarized in Charters et al. (2015)……24

Figure 7. SEM images of the five TWP types (Park et al., 2018)……25

Figure 8. Fate processes for microplastic in the riverine system. (Black arrows represent processes incorporated in ePLAS model, while the white arrows indicate processes will be added in later stage)……28

Figure 9. A schematic diagram of different environmental compartments including fate processes (using the START point as an example). Note: the ETWP referred to in the diagram represents the point source or diffuse source emissions discussed in the previous chapter……35

Figure 10. A schematic diagram of different environmental compartments including fate processes (Starting at the second node after the START node). Note: the ETWP referred to in the diagram represents the point source or diffuse source emissions discussed in the previous chapter……38

Table 1. River parameter……17

Table 2. Estimated per capita emission of different categories of microplastics by the Dutch population (Sun et al., in prep.)……18

Table 3. European WWT coverage and estimated average microplastic retention rates. Source: Eunomia (2018), Data extrapolated from Eurostat from latest reported data from each country (2009—2013, 2005 for Cyprus)..20

Table 4. Size distribution of TWP used in the present model (base on Kreider et al., 2010)……25

Table 5. Morphologies of tyre materials obtained under various sampling conditions……26

Table 6. Density distribution of TWP in literatures……27

Table 7. Parameterization for TWP in our study……28

Table 8. Parameterization for SPM in our study……33

Table S1. Rate constants of processes in the model……39

## ABBREVIATIONS AND ACRONYMS

| Abbreviation / Acronym | Description |
|---|---|
| **ePiE** | exposure to Pharmaceuticals In The Environment |
| **ePLAS** | Emission of MicroPLAStics To The Envrioment |
| **SPM** | Suspended Particulate Matter |
| **TRWP** | Tyre and Road Wear Particles |
| **TWP** | Tyre Wear Particles |
| **WWTP** | Waste Water Treatment Plant |

## PREFACE

This report provides a technical description of the ePLAS model, i.e. a network model that aims to describe the fate of microplastics in European rivers and lakes. It is the result of Task 7.1 of the LABPLAS project, called Source-to-Ocean Model. The aim of this task was to develop an infrastructure for a European PLastic informAtion System (ePLAS). The original title of this deliverable (D7.1) was "Technical report describing the ePLAS model, including case studies for the Elbe, Thames and Mero-Barcés river basins". Deliverable 7.1 will be followed by a second deliverable, i.e., D7.2, entitled "Guideline for parameterizing and operationalizing ePLAS for Europe".

As the title of D7.1 indicates, our initial intention was to include case studies on the Elbe, Thames and Mero-Barcés river basins in this technical report. However, we decided that these case studies would better fit in D7.2 since then the user can actually see how we applied the ePLAS model to these three case study areas. Hence, the case studies on the Elbe, Thames and Mero-Barcés river basins are not included in this technical report, but instead will be included in D7.2 which is scheduled to be delivered in M46 (March 2025).

The current version of the ePLAS model focuses on the fate of microplastics in river water and sediments. Initially, we aimed to expand our river model to the estuary and ocean and include other fate processes such as bioaccumulation and deposition of microplastics from air. This is Milestone 23 of the LABPLAS project description. We discussed the options with other WP7 partners and concluded that the modelling concepts currently applied for estuaries, oceans, bioaccumulation and exchange with air (i.e., dynamic process formulations) are incompatible with the steady-state assumption applied in the ePLAS model. It was therefore decided not to include these compartments and processes in the current version of the ePLAS model. As explained below, in a later stage, we intend to refine and further expand the ePLAS model once the current model structure and process formulations have been implemented and tested. We will then also explore whether a dynamic version of the model can be deloped. Once this step has been taken, we can consider to expand the model with a module for estuaries and oceans, and include fate processes like bioaccumulation and deposition of microplastics from air.

The author team

# 1 INTRODUCTION

APIs are widely used and typically not completely metabolized during passage through the human body and wastewater treatment plants (WWTPs), resulting in partial entry into the environment. Pharmaceutical residues primarily enter the environment through the effluent of WWTPs. Although reported concentrations are generally low, i.e., in the ng/L to µg/L range (aus der Beek et al., 2015; Fatta‐Kassinos et al., 2011; Kümmerer, 2010), certain pharmaceuticals may pose ecological risks due to their specific modes of action and high potency.

The ePiE (exposure to Pharmaceuticals in the Environment) model, initially developed by Oldenkamp et al. (2013), has been designed to estimate concentrations of active pharmaceutical ingredients (APIs) in European surface waters. This model uses national consumption data of pharmaceuticals to provide spatially explicit estimates of pharmaceutical concentrations across various aquatic compartments, i.e. surface water and sediment. The ePiE model effectively captures the transition of these compounds from emission at the point of consumption through various environmental fate processes, ultimately estimating their long-term (yearly) average steady-state concentrations in surface waters and sediments post-WWTP treatment.

The ePiE model follows a structured methodology from emission and fate in the aquatic environment to exposure. It starts by calculating the emission of APIs into wastewater, attributing it to factors such as patient non-compliance and subsequent disposal (e.g., through flushing), as well as the actual consumption and excretion as the parent compound in urine and faeces. The pharmaceutical residues are then distributed to various urban agglomerations based on population size. Depending on the level of WWTP connectivity, wastewater from partially or completely unconnected urban agglomerations may be directly discharged into surface waters. Additionally, the ePiE model uses regressions to estimate local, year-specific flow metrics (annual average, minimum, and maximum monthly flow). Combined with spatially explicit information on the location and characteristics of WWTPs throughout Europe, this enables the prediction of concentrations in surface waters at specific coordinates. Furthermore, because it performs directed calculations through the river network, ePiE incorporates the contribution of upstream sources in the assessment of individual WWTPs. This approach offers advantages over traditional process-based hydrological models, which can be time-consuming and data-intensive and not always provide the ability to pinpoint locations of interest.

However, the urgency of environmental concerns is not confined to pharmaceuticals alone. Microplastic pollution of aquatic ecosystems has emerged as a parallel and pressing issue. Microplastics have been identified in nearly all aquatic environments, from marine ecosystems to river systems, polar regions, and even deep ocean environments (Rowley et al., 2020; Sarkar et al., 2021; Fragão et al., 2021; Cunningham et al., 2020), and may pose a threat to those systems. The large amount of microplastics found in marine environments are traced back to land-based sources, underscoring the role of rivers as critical conduits for the transport of these pollutants from terrestrial to aquatic environments (Morales-Caselles et al., 2021). Indeed, the ePiE model is precisely a high-resolution model for the transport of environmental pollutants across river and lake networks, providing a suitable infrastructure to simulate the fate of microplastics.

Given the similarities between pharmaceuticals and microplastics as environmental pollutants and the current lack of large-scale, high-resolution models for microplastic transport, there is a compelling rationale to adapt the existing ePiE framework to simulate the transport of microplastic particles within river and lake systems. Due to the unique physical properties of microplastics, their transport processes do not fully align with those of APIs as included in the ePiE model. For instance, microplastics originate from a wide range of sources (e.g., tyre wear, pellets, microfibers, etc.) and cannot be simplified to a single uniform size or shape. Notably, particles from tyre wear, which constitute a significant source of microplastic pollution (Wagner et al., 2018), are typically

ellipsoidal in shape. In contrast, tiny microplastic fibers tend to be cylindrical. Beyond the differences in shape, the size of microplastic particles also varies widely, i.e. from the nm-range to the mm-range. Particles from different sources exhibit distinct size distributions and, similarly, the polymer types and densities may vary. In addition to these inherent unique physical properties, microplastics in river environments interact with suspended particulate matter (SPM) and microbial communities. These factors significantly influence the transport dynamics and distribution patterns of microplastics in river systems, which is crucial for identifying potential hotspots and developing strategies to reduce microplastic accumulation in rivers.

This report describes the adaptation of the original process formulations of the ePiE model to enable the prediction and assessment of microplastic concentrations in European rivers, lakes and sediments. By utilizing the high spatial resolution (~1x1 km) and comprehensive data integration capabilities of the ePiE model, the updated model (ePLAS) aims to capture the complex transport dynamics of microplastics across extensive geographic areas, with the aim to provide insight into their environmental dispersion and potential impacts. This adaptation not only extends the utility of the ePiE model but also enhances our capacity to address an emerging environmental challenge with significant ecological and health implications.

This technical manual primarily differs from the original ePiE model's technical description (Oldenkamp et al., 2018) in that it focuses exclusively on microplastic particles. Chapter 2 revisits the original structure of the ePiE model along the lines of a multimedia box model, explaining how different boxes are distinguished for improved analysis of microplastic behavior in riverine environments. Chapter 3 describes the derivation of some key hydrological parameters essential for modeling microplastics in rivers and lakes. Chapter 4 outlines the methods for quantifying microplastic emissions, incorporating per capita emissions data with wastewater treatment coverage and efficiency to correctly allocate emissions across river segments. Chapter 5 details how microplastics from different sources are defined across dimensions (size, shape, and density) to simulate their transport in aquatic environments. Finally, Chapter 6 traces the fate processes of microplastics once they enter into aquatic systems, establishing mass conservation equations under steady-state conditions of microplastics.

## 2 MODELLING CONCEPT

ePiE is a network model representing a system of connected rivers and lakes (Figure **2**). It consists of dots (nodes) which are typically 1 km apart and which can represent different system elements, e.g., a river stretch, a WWTP, a confluence, a bifurcation or a lake. Directed calculations are performed based on API loads that are discharged from WWTPs and transported from one node to the next. Dissipation processes are currently modelled based on the average time it takes the water to flow from one node to the next.

The ePiE modelling concept works fine for predicting API concentrations in the water compartment under the assumption of constant water flow, WWTP discharge(s) and related fate and dissipation processes, but cannot be used for modelling (dynamic) fate processes between multiple compartments, i.e. water and sediment. The exchange of microplastics between the water column and sediment changes over time with the build-up of microplastic concentrations in the sediment. These dynamics can theoretically be simulated by applying a time loop to the ePiE model (i.e., repeating the calculations for finite time steps), but this requires substantial computational time. Furthermore, given the fact that water flow and pollutant discharge are currently assumed constant, this would ultimately result in a steady-state situation.

A multimedia box model approach can be used to simulate fate processes in multiple compartments. Multimedia box models were first introduced by Mackay (1991). In these models, the environment is represented by a limited number of boxes, such as soil, water and air, and the exchange processes between these boxes are captured in a set of differential equations, i.e., one for each box. The differential equations can be solved for different situations (or levels), with level 3 representing the steady-state situation, i.e., a situation of dynamic equilibrium which is typically obtained when emissions and flows are constant. This option is chosen here to simulate the fate of microplastics with ePLAS, i.e., each river stretch between two consecutive nodes is represented by three boxes, i.e., the water layer, the bed load layer and the sediment layer (Figure **2**) that are assumed to be in a dynamic equilibrium.

It should be noted that the assumption of a dynamic equilibrium is debatable for river systems which are typically characterized as highly dynamic systems. Continuous temporal changes in water flow (and pollutant discharges) are likely to result in fluctuations impeding the system to reach a steady-state. Nonetheless, the steady-state assumption will initially be applied for ePLAS to obtain a first impression of the fate of microplastics in European riverine systems. Once the steady-state model has been established, it will be explored whether it is feasible to turn the model into a dynamic model. The availability of temporal data on water flow and microplastic discharges, as well as computational considerations (i.e., the time step versus the computational time required to run the model), will play an important role in this future refinement.

This report describes how the multimedia box model approach is integrated into the ePiE model in order to simulate the fate of microplastics. This is illustrated in Figure **2**, where each pair of adjacent river nodes is considered as a river stretch consisting of three interrelated boxes, i.e., a water layer, a bed load layer and a sediment layer. As shown in Figure **1**, different fate processes occur within and between the compartments, including advective transport between boxes such as transport of water and bed load transport (sediment). It also encompasses the heteroaggregation of microplastic particles with suspended particulate matter within the water compartment. Additionally, processes of sedimentation and resuspension occur between the water layer and bed load layer. Burial transports sediment particles and microplastics from the bed load layer into the sediment, but also results in dissipation from the sediment layer (into deep layers and out of the system).

The dimensions of the river stretch between two nodes can vary, including the width and depth of the river. These dimensions will be introduced in Section **3.2**. The various fate processes mentioned above will be detailed in Section **6**.

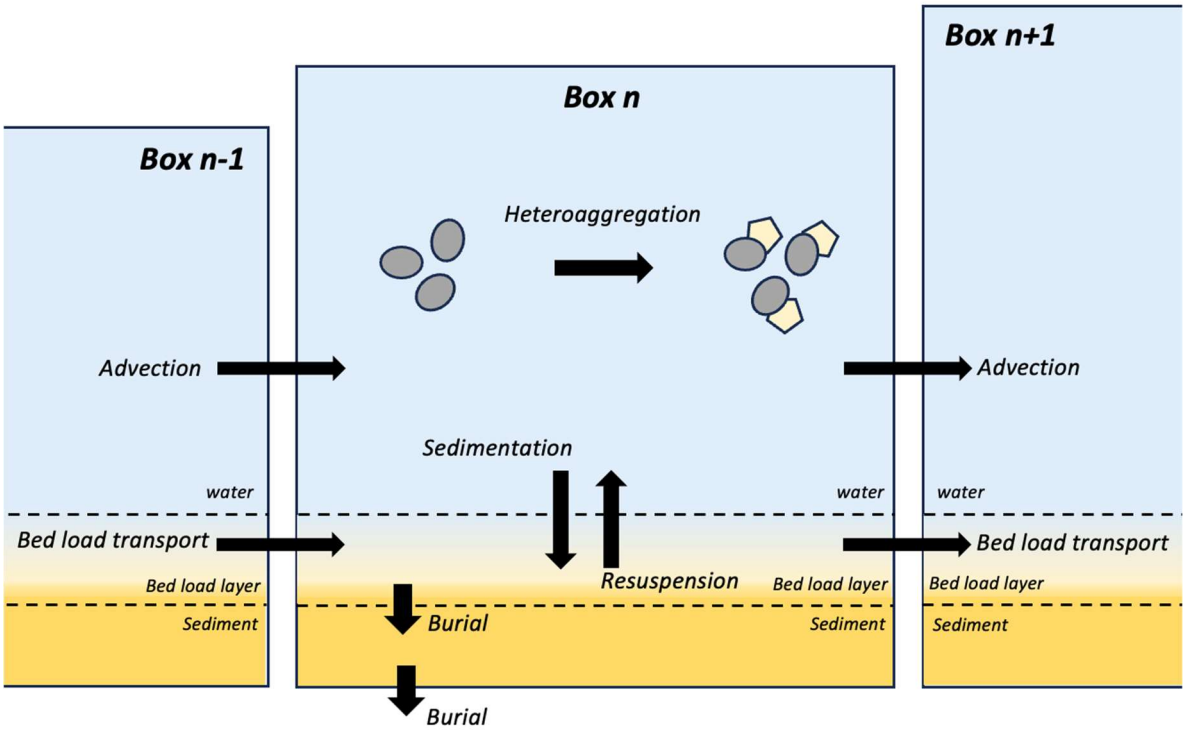


*Figure 1. Fate processes of microplastics in the water layer, bed load layer and sediment layer.*

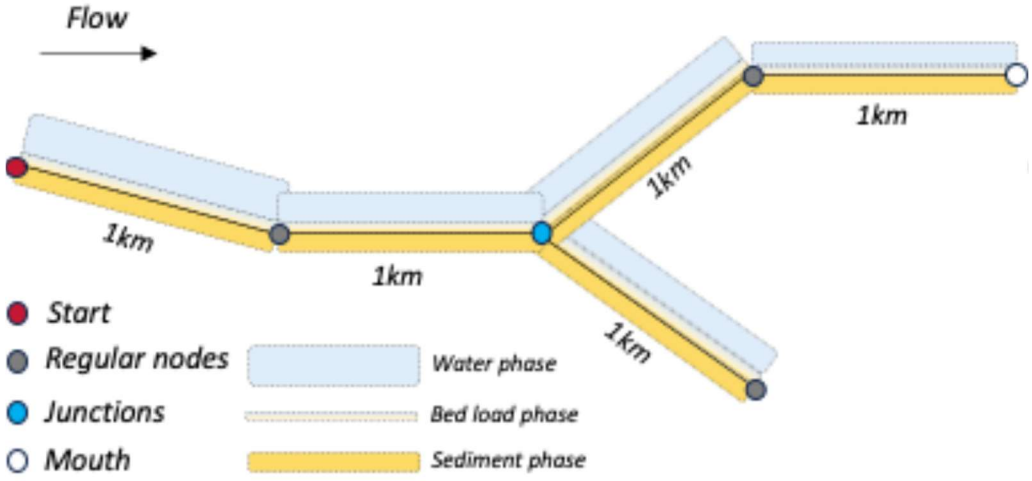


*Figure 2. Applying the multimedia box model to river nodes schematic diagram.*

## 3 HYDROLOGY OF RIVERS AND LAKES

For a location-specific estimation of microplastic concentrations, the ePLAS model requires hydrological characteristics such as river discharge volumes (Q; m³/s), river flow velocities (v; m/s), and river depth (Hw; m). For lakes and reservoirs, necessary data include the hydraulic retention time (HRT; s) and lake depth (H; m). This chapter first summarizes how the FLO1K dataset, which provides high-resolution river flow metrics globally using artificial neural network regressions, was initially integrated into the original ePiE model, allowing accurate assignment of discharge data to each river node. Additionally, it provides a detailed explanation of how important hydrological parameters, such as river flow velocity and river depth, are being derived from these discharge data.

***River discharge volume Q***

In the ePLAS model, year-specific flow data are automatically assigned to the nodes in the river network based on the year and flow conditions selected by the user. For characterizing annual mean flow, and the highest and lowest monthly mean flow, the global FLO1K dataset (Barbarossa et al., 2018) is incorporated into ePLAS. FLO1K relies on an ensemble of artificial neural network regressions, with upstream-catchment physiography (area, slope, elevation) and year-specific climatic variables (precipitation, temperature, potential evapotranspiration, aridity index, and seasonality indices) as covariates. It offers estimations of flow at a spatial resolution of 30 arc seconds (~1x1 km) for the years 1960-2015, aligning well with independent data (global $R^2$ of single-year metrics up to 0.91). A further comparison with independent data from 1,007 European monitoring stations for the period 2010-2015 (GRDC, 2015) indicated that the model accurately predicts year-specific annual mean flow, and highest and lowest mean monthly flow in European rivers, with $R^2$ values of 0.97, 0.95, and 0.91, respectively (Figure **3**).

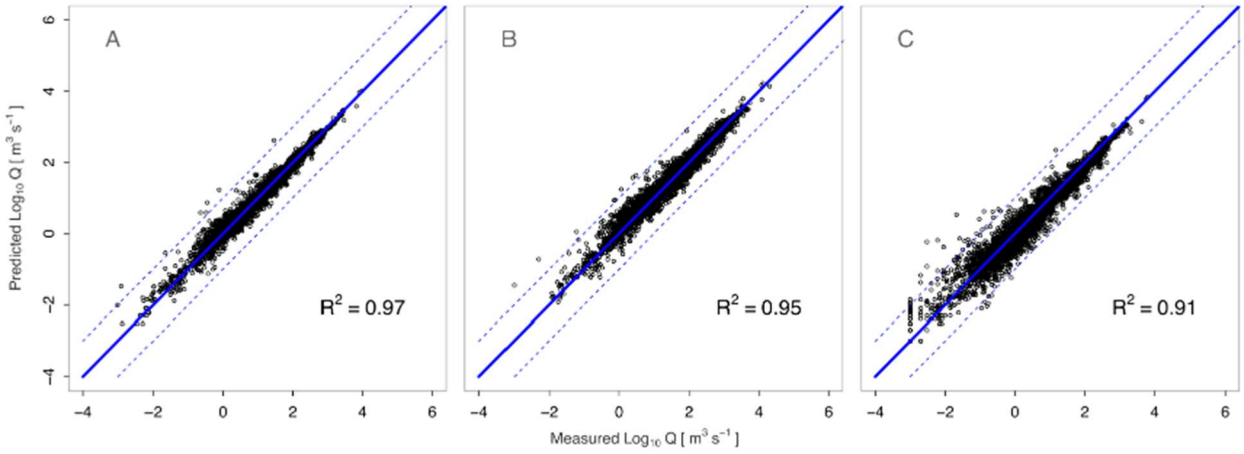


*Figure 3. Validation results of river discharge volume for year-specific annual mean (A), maximum (B), and minimum (C) monthly flow conditions. Independent validation dataset consisted of yearly measurements from 2010 to 2015 at 1,007 GRDC European stations. The solid line represents a perfect model fit (1:1 line), and the dashed lines indicate a difference of one order of magnitude.*

***River flow velocity v and river depth Hw***

River flow velocity is commonly estimated with the widely used Manning-Strickler equation for open channel flow (Equation **1**) (e.g., Pistocchi and Pennington, 2006; Schulze et al., 2005).

$$v_w = \frac{R^{2/3} \cdot S^{1/2}}{n} \qquad Equation\ 1$$

where,

v = the river's flow velocity (m/s);

R = the hydraulic radius of the river (m);

S = the river slope (m/m);

n = the river bed roughness (s/m³).

The Manning-Strickler equation makes use of the hydraulic radius R, which is defined as the ratio of the cross-sectional area A (m²) over the wetted perimeter P (m): R=A/P. For estimation of this hydraulic radius R, it is often assumed that the river bed is shaped as a rectangle. Moreover, since the depth of the river's water column Hw (m) is generally much smaller than the width of the river (W; m), especially for major rivers, R can be approximated by depth (Pistocchi and Pennington, 2006):

$$R = \frac{A}{P} \approx \frac{H_w \cdot W}{2 \cdot H_w + W} \approx \frac{H_w \cdot W}{W} = H_w \qquad Equation\ 2$$

where,

A = the cross-sectional area of the river (m²);

P = the wetted perimeter of the river (m);

Hw = the depth of the river's water column (m);

W = the width of the river (m).

Additionally, the assumption of a rectangular river bed means that the flow velocity v is related to the discharge volume Q, river depth Hw, and river width W (Equation **3**), enabling the calculation of river depth via Equation **4**.

$$v_w = \frac{Q}{A} = \frac{Q}{H_w * W} \qquad Equation\ 3$$

$$H_w = \frac{Q}{v_w * W} \qquad Equation\ 4$$

Thus, R in the Manning-Strickler equation (Equation **1**) can be substituted by the term $\frac{Q}{v_w * W}$, resulting in Equation **5**.

$$v_w = n^{-\frac{2}{3}} * Q^{\frac{2}{5}} * W^{-\frac{2}{5}} * S^{\frac{3}{10}} \qquad Equation\ 5$$

Consequently, in order to estimate flow velocity v, four parameters are required: river discharge volume Q, river width W, river bed roughness n, and river slope S (m/m). For Q, we used location specific estimations via the spatial regression model described above, and for S we used the HydroSHEDS Digital Elevation Map (DEM) at 3 arc-seconds resolution (Lehner et al., 2008a).

For the other two parameters, i.e. river width W and river bed roughness n, continuous spatially explicit data are generally not available. Andreais et al. (2013) calculated width and depth for all streams in the HydroSHEDS database. However, they used relatively poor estimations of discharge, and one overall global equation describing the relationships between discharge and width and between discharge and depth, without any spatial differentiation. Since the relationship between discharge and river dimensions varies spatially, we applied Equation **6** for river width of European rivers specifically, as derived by Pistocchi and Pennington (2006) ($r^2$=0.868). They based this regression on 186 river width measures across the European continent covering a range of ~10 m to ~1000 m.

$$W = 7.3607 \cdot Q^{0.52425} \qquad Equation\ 6$$

In addition to a European average equation, Pistocchi and Pennington (2006) also derived regional equations for specific river catchments in Europe. However, the spatial extent of these regressions (i.e., where does which regression apply), does not become clear from the reported information. They are merely indicatively described (e.g., "East of the Rhine"), and therefore not usable for the ePLAS model.

Values for Manning's roughness coefficient n in natural streams generally vary between 0.015 s/$m^{1/3}$ and 0.07 s/$m^{1/3}$ for flows with less than bankfull discharge. They can reach up to 0.25 s/ $m^{1/3}$ for overbank flows (Schulze et al., 2005). Very few local data exist, and assessing local river bed roughness throughout Europe is currently considered infeasible. Based on Pistocchi and Pennington (2006), we applied an overall value for n of 0.045 s/ $m^{1/3}$. This value represents optimality: using it ensures that errors on the estimated velocity are maximally limited, and approximately within ±40% for any "true" value of n that might occur locally.

| *Parameter* | *Symbol* | *Value* | *Unit* | *Reference* |
|---|---|---|---|---|
| *River discharge volume* | *Q* | - | *$m^3$/s* | *Barbarossa et al., 2018* |
| *Distance between river nodes* | *dist_nxt* | - | *m* | |
| *River flow velocity* | *$v_w$* | $v_w = n^{-\frac{2}{3}} * Q^{\frac{2}{5}} * W^{-\frac{2}{5}} * S^{\frac{3}{10}}$ | *m/s* | *Pistocchi and Pennington, 2006; Schulze et al., 2005* |
| *River width* | *W* | $W = 7.3607 \cdot Q^{0.52425}$ | *m* | *Andreais et al. 2013* |
| *River depth* | *$H_w$* | $H_w = \frac{Q}{v * W}$ | *m* | *Pistocchi and Pennington., 2006* |
| *Local water temperature* | *$T_w$* | *285* | *K* | *Markovic et al., 2013* |
| *Dynamic Viscosity of fluid at 11.4℃* | *$\mu_w$* | *0.001255* | *kg/m* s* | |
| *Volume of water in box n of the river sediment* | *$V_{w,n}$* | *dist_nxt * $H_w$* W* | *$m^3$* | |

| | | | | |
|---|---|---|---|---|
| *Density of suspending medium water, at 11.4℃* | $\rho w$ | *0.9996* | $g/cm^3$ | |
| *Gravitational acceleration on earth* | $g$ | *9.81* | $m/s^2$ | |
| *Mixed depth of sediment column relevant for exchange* | $H_{sed}$ | *0.02* | *m* | *Praetorius et al., 2012* |
| *Boltzmann constant* | $k_B$ | *1.38E-23* | *J/K* | |
| *Density of sediment* | $\rho_{sed}$ | *2.5* | $g/cm^3$ | *Praetorius et al., 2012* |
| *Porosity of the sediment* | $\Phi_{sed}$ | *0.85* | - | *Praetorius et al., 2012* |
| *Velocity of sediment transfer (bed load shift)* | $v_{sed\_transfer}$ | *3.00* | *kg/s* | *Praetorius et al., 2012* |
| *Volume of sediment in box n of the river sediment* | $V_{sed,n}$ | *dist_nxt * $H_{sed}$ * $W_w$* | $m^3$ | |
| *Mass of sediment in box n of the river sediment* | $m_{sed,n}$ | *(1-Φsed) * $\rho_{sed}$ * $V_{sed,n}$* | *kg* | |

*Table 1. River parameters*

# 4 EMISSION ESTIMATION

This chapter begins by determining the per capita emissions for different sources of microplastics to align with the ePLAS model. It then introduces Sections **4.2** and **4.3**, which describe how per capita emissions are combined with WWTP population connectivity and microplastic treatment efficiency. Finally, Section **4.4** focuses on the specific allocation methods that were adopted for point source and diffuse source emissions, respectively.

## 4.1 Per capita emission

Unlike APIs, where the estimation of emissions requires consumption data of drugs (or their precursors) and adjustments based on the proportions of the drug excreted through urine and faeces, the estimation of microplastic emissions, due to their diverse sources, necessitates establishing detailed methods for each source and distinct emission pathways across different environmental compartments.

ePLAS addresses seven key sources of riverine microplastic pollution: tyre wear, textile fibers, pellets, architectural paints, road markings, marine paints, and scrubbing agents. To ensure that emission data fully align with administrative/political boundaries as well as hydrological boundaries and sewage service areas, the model requires per capita emissions for each country. This approach is necessary because factors like GDP per capita vary significantly between countries, influencing the amount of microplastic emissions from sources such as tyre wear. As an example, Table **2** presents the estimation of the annual per capita emissions of various types of microplastics by individuals in the Netherlands (Sun et al., in prep.). The emissions vary significantly across different microplastics categories, from as low as 0.003 kg/year per capita for marine paints to as high as 1.52 kg/year per capita for tyre wear. In order to run ePLAS for microplastics, it requires an estimate of the national per capita emission for each of the microplastics categories analyzed and for each of the countries which are part of the geographical area studied (i.e., the river basins).

| MP Sources | Tyre wear | Pellets | Textile fibers | Architectural paints | Scrubbing agents | Road marking | Marine paints |
|---|---|---|---|---|---|---|---|
| Per capita emission [kg/y*cap] | 1.52 | 0.22 | 0.05 | 0.05 | 0.019 | 0.007 | 0.003 |

*Table 2. Estimated per capita emission of different categories of microplastics by the Dutch population (Sun et al., in prep.)*

## 4.2 European wastewater treatment plants and agglomerations

In our study, wastewater treatment plant (WWTP) data are sourced from the HydroWASTE database, a spatially explicit global compilation of 58,502 WWTPs. HydroWASTE was developed by integrating national and regional datasets with supplementary information to complete missing data points, enhancing the robustness of our environmental assessments. This database supports the ePLAS model by detailing locations, waste loads entering, and connection percentages of agglomerations to WWTPs, essential for assessing the distribution and characteristics of agglomerations and their associated wastewater systems. Each WWTP is documented with its geographic coordinates, incoming load, design capacity, and the level of treatment provided, ranging

from primary to advanced treatments such as nitrogen removal, phosphorus removal, chlorination, ozonation, UV treatment, and sand filtration.

The database utilizes the HydroSHEDS river network and streamflow estimates to geo-reference the outfall locations of WWTPs, ensuring accurate alignment with the global river network provided by the HydroRIVERS database. This alignment is crucial for analyzing the distribution and impact of wastewater on a global scale. By integrating the per capita annual emissions of various microplastic types with the population density of catchment areas linked to each WWTP and their operational efficiencies, the database allows us to compute the annual microplastic emissions for each point source. It ensures that our calculations of annual microplastic emissions and other pollutants from point sources are based on precise and comprehensive WWTP characteristics and their operational efficiencies.

### 4.3 Fate during wastewater treatment

In the original ePiE model, after APIs are consumed and subsequently excreted, the wastewater containing these compounds may be directed to a wastewater treatment plant (WWTP). In environmental risk assessments of pharmaceuticals, the removal rate of APIs within WWTPs is typically assessed either through literature review of full-scale measurements or by employing predictive models. The SimpleTreat 4.0 model was implemented to simulate the chemical fate in WWTPs, focusing on processes such as partitioning and degradation in activated sludge systems.

Unlike APIs, the fate of microplastics in WWTPs differs significantly, which is why the SimpleTreat 4.0 model was not used in the updated ePLAS model to calculate the removal efficiencies of microplastics across different levels of wastewater treatment plants. Additionally, given the diverse sources of microplastics, which correlate to varying densities, sizes, and shapes, it is currently impractical to include this level of complexity by studying each category of microplastics separately. Consequently, this report temporarily adopts the coverage and microplastic removal efficiencies of WWTPs across all EU member states as discussed in the Eunomia report (Table **3**).

LABPLAS

Horizon 2020
European Union Funding
for Research & Innovation

| Proportion of Population Covered by WWT Type (Eurostat) | | | | | | | | | Average Microplastic Retention fraction by WWT Type and Converge | | | | | | | |
|---|---|---|---|---|---|---|---|---|---|---|---|---|---|---|---|---|
| **Country** | P | S | T | NS | IND | TT | UKN | Σ | P | S | T | NS | IND | TT | UKN | Avg |
| **Netherlands** | - | - | 99% | - | 1% | - | - | 100% | - | 0.2% | 85.1% | - | 0.5% | - | - | 86% |
| **Malta** | - | 6% | 92% | - | - | 1% | - | 100% | - | 4.1% | 79.1% | - | - | 0.7% | - | 84% |
| **Germany** | - | 3% | 93% | 1% | 3% | - | - | 100% | - | 1.9% | 79.8% | 0.5% | 1.5% | - | - | 84% |
| **Austria** | - | 1% | 94% | - | 6% | - | - | 100% | - | 0.6% | 80.3% | - | 2.8% | - | - | 84% |
| **Switzerland** | - | 11% | 87% | - | 2% | - | 0.3% | 100% | - | 7.0% | 74.7% | - | 0.9% | - | - | 83% |
| **Denmark** | 1% | 2% | 88% | - | 9% | - | 0.1% | 100% | 0.4% | 1.2% | 75.7% | - | 4.6% | - | - | 82% |
| **Sweden** | - | 4% | 83% | - | 13% | - | - | 100% | - | 2.5% | 71.3% | - | 6.5% | - | - | 80% |
| **Finland** | - | - | 83% | - | 17% | - | - | 100% | - | - | 71.3% | - | 8.5% | - | - | 80% |
| **Luxembourg** | 2% | 27% | 70% | - | 2% | - | - | 100% | 0.9% | 16.8% | 59.9% | - | 0.9% | - | - | 79% |
| **Greece** | - | 6% | 86% | - | - | - | 7.9% | 92% | - | 4.0% | 73.7% | - | - | - | - | 78% |
| **Spain** | 1% | 28% | 67% | 2% | 1% | - | 1.3% | 99% | 0.3% | 17.8% | 57.3% | 1.2% | 0.5% | - | - | 77% |
| **Belgium** | - | 11% | 73% | - | 11% | - | 5.0% | 95% | - | 7.0% | 62.7% | - | 5.5% | - | - | 75% |
| **UK** | - | 50% | 50% | - | - | - | 0.4% | 100% | - | 31.5% | 42.8% | - | - | - | - | 74% |
| **Estonia** | - | 5% | 77% | - | 5% | - | 12.8% | 87% | - | 3.2% | 66.2% | - | 2.5% | - | - | 72% |
| **Norway** | 19% | 1% | 61% | - | 15% | - | 3.0% | 97% | 9.2% | 0.9% | 52.5% | - | 7.6% | - | - | 70% |
| **Poland** | - | 14% | 56% | - | - | 25% | 4.8% | 95% | - | 9.0% | 48.1% | - | - | 12.5% | - | 70% |
| **Czech Republic** | - | 8% | 72% | - | 2% | - | 17.6% | 82% | 0.1% | 5.2% | 61.5% | - | 1.2% | - | - | 68% |
| **Latvia** | 4% | 50% | 17% | - | 29% | - | 0.1% | 100% | 1.8% | 31.8% | 14.8% | 0.2% | 14.5% | - | - | 63% |
| **Lithuania** | - | 2% | 61% | 11% | - | 7% | 18.8% | 81% | - | 1.5% | 52.1% | 5.5% | - | 3.6% | - | 63% |

| | | | | | | | | | | | | | | | | |
|---|---|---|---|---|---|---|---|---|---|---|---|---|---|---|---|---|
| **France** | 1% | 33% | 22% | 25% | 19% | - | - | 100% | 0.4% | 21.1% | 19.0% | 12.6% | 9.3% | - | - | 62% |
| **Ireland** | - | 47% | 18% | - | 31% | - | 4.0% | 96% | - | 29.8% | 15.5% | - | 15.5% | - | - | 61% |
| **Hungary** | - | 16% | 57% | - | - | - | 27.3% | 73% | - | 10.2% | 48.5% | - | - | - | - | 59% |
| **Cyprus** | - | 12% | 18% | - | 70% | - | - | 100% | - | 7.3% | 15.7% | - | 35.1% | - | - | 58% |
| **Slovenia** | 1% | 33% | 22% | - | 35% | - | 9.4% | 91% | 0.2% | 21.1% | 18.6% | - | 17.6% | - | - | 58% |
| **Bulgaria** | 2% | 19% | 35% | - | 25% | - | 18.2% | 82% | 0.9% | 12.3% | 30.3% | - | 12.7% | - | - | 56% |
| **Croatia** | 16% | 36% | 1% | - | 45% | - | 1.7% | 98% | 7.6% | 22.8% | 0.9% | - | 22.7% | - | - | 54% |
| **Slovakia** | - | - | - | 62% | 36% | - | 1.6% | 98% | - | - | - | 31.0% | 18.2% | - | - | 49% |
| **Italy** | 3% | 22% | 35% | - | 5% | - | 35.0% | 65% | 1.4% | 14.0% | 30.0% | - | 2.5% | - | - | 48% |
| **Portugal** | 4% | 39% | 16% | 11% | - | - | 29.3% | 71% | 1.7% | 25.0% | 14.1% | 5.7% | - | - | - | 46% |
| **Romania** | 9% | 18% | 18% | - | 4% | - | 51.3% | 49% | 4.2% | 11.1% | 15.5% | - | 2.2% | - | - | 33% |
| | | | | | | | **Maximum Retention Rates by Technology** | | 78% | 98% | 99.70% | 50% | 50% | 50% | 0% | - |
| | | | | | | | **Minimum Retention Rates by Technology** | | 17% | 29% | 72% | 50% | 50% | 50% | 0% | - |

*Table 3. European WWT coverage and estimated average microplastic retention rates. Source: Eunomia (2018), Data extrapolated from Eurostat from latest reported data from each country (2009—2013, 2005 for Cyprus)*

*Notes:*

*(1) P = Primary wastewater treatment: Treatment of wastewater by a physical and/or chemical process involving settlement of suspended solids, or other process in which the Biochemical Oxygen Demand (BOD5) of the incoming wastewater is reduced by at least 20% before discharge and the total suspended solids of the incoming wastewater are reduced by at least 50%.*

*(2) S = Secondary wastewater treatment: Post-primary treatment of wastewater by a process generally involving biological treatment with a secondary settlement or other process, resulting in a Biochemical oxygen demand (BOD) removal of at least 70% and a Chemical Oxygen Demand (COD) removal of at least 75%. Natural biological treatment processes are also considered under secondary treatment if the constituents of the effluents from this type of treatment are similar to the conventional secondary treatment.*

*(3) T = Tertiary wastewater treatment: Treatment (additional to secondary treatment) of nitrogen and/or phosphorous and/or any other pollutant affecting the quality or a specific use of water: microbiological pollution, color etc. The different possible treatment efficiencies ('organic pollution removal' of at least 95% for BOD5, 85% for COD, 'nitrogen removal' of at least 70%, 'phosphorous removal' of at least 80% and 'microbiological removal') cannot be added and are exclusive.*

*(4) NS = Not Specified: Other wastewater treatment corresponds to treatment of wastewater in any non-public treatment plant, i.e., Industrial Wastewater Treatment Plants (IWWTPs). Excluded from "other wastewater treatment" is the treatment in septic tanks. IWWTPs may also be classified under ISIC 37 (Sewerage) or under the main activity class of the industrial establishment they belong to.*

*(5) IND = Independent: Facilities for preliminary treatment, treatment, infiltration or discharge of domestic wastewater from dwellings generally between 1 and 50 population equivalents, not connected to an urban wastewater collecting system. Examples of such systems are septic tanks.*

*(6) TT = Truck Transported: Systems with storage tanks from which the wastewater is transported periodically by trucks to an urban wastewater treatment plant.*

*(7) UKN = Unknown/no treatment: wastewater which doesn't undergo any form of treatment before discharge to the environment.*

## 4.4 Allocation of emissions to river nodes

### 4.4.1 Types of river nodes

The river networks in ePLAS were constructed for individual watersheds delineated in the global database HydroSHEDS (Lehner et al., 2008b). For each watershed, the river network was cropped at a resolution of 30 arcseconds (~1x1 km) using its boundaries, which were derived from the HydroSHEDS database, and converted to a binary 30 arcsecond raster containing information on the presence or absence of river elements. The raster cells containing river elements were then used to create a spatial point file, with each point representing a network node. All nodes were automatically categorized as (Figure **4**):

1. Start (node representing the source of a river);

2. Mouth (nodes where a river flows into the sea);

3. Junctions (nodes where two streams meet, with two upstream nodes);

4. Regular nodes;

5. WWTP/Agglomeration discharge points (nodes representing the point source to the river).

Typically, the first four types of river nodes are spaced approximately 1 km apart. However, the fifth type, WWTP/Agglomeration nodes, usually represents urban population centers and is therefore often situated along the river stretches between the aforementioned nodes, rather than strictly adhering to the 1 km interval (Figure **4**). This placement reflects the practical location of wastewater treatment plants and agglomerations relative to river configurations.

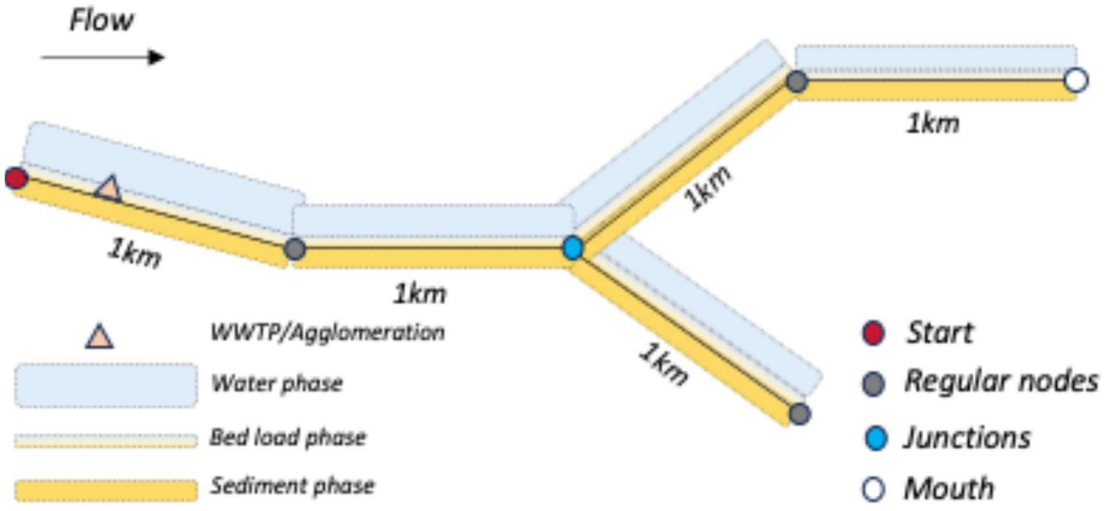


*Figure 4. Schematic diagram of river nodes for different types (WWTP/Agglomeration will be added to the ePLAS model as a point source)*

### 4.4.2 Point sources and diffuse sources

Microplastics can enter surface waters either via a sewer system (often via a WWTP) or through direct emission (e.g., runoff). In our model, the former is defined as a point source, whereas the latter is categorized as a diffuse source.

(1) For point sources, the calculation begins by using the per capita emission rate of an EU member state as presented in Table **1**, followed by determining the proportion entering WWTPs (i.e., the part of the

emissions that is treated in a WWTP as part of the environmental pathway segmentation) (Sun et al., prep). This is then combined with the population served by the corresponding WWTP, and multiplied by the average microplastic removal efficiency for the respective EU member state as indicated in Table **2**. The final result represents the point source emission from a WWTP into the river network for that specific point (Equation **7**).

$$E_{point} = E_{cap,p} \cdot F_{WWTP} \cdot F_{Inh} \cdot F_{Removal} \qquad Equation\ 7$$

where,

$E_{point}$ = the point source emissions entering the river network via WWTPs (kg/y);

$E_{cap,p}$ = the per capita microplastic emission to WWTPs for a particular EU member state (kg/cap*y);

$F_{WWTP}$ = the proportion of wastewater treated in WWTPs for a certain EU member state (%);

$F_{Inh}$ = the number of inhabitants connected to a specific WWTP node (-);

$F_{Removal}$ = the average microplastic removal efficiency for certain EU member states (%).

(2) For diffuse sources, which represent direct emissions into surface waters, emissions are allocated based on the proportion of each river stretch in the length of the total river network. First, the total national diffuse emission is calculated, and then this value is multiplied by the proportion of a specific river stretch length relative to the total river network length in the country to determine the emission taking place in that segment (Equation **8**).

$$E_{diffused} = E_{cap,d} \cdot F_{population} \cdot \frac{L_{WWTP}}{L_{Total}} \qquad Equation\ 8$$

where,

$E_{diffused}$ = the diffused source emissions entering the river network directly (kg/y);

$E_{cap,d}$ = the per capita microplastic emission from diffuse sources for a particular EU member state (kg/cap*y);

$F_{population}$ = the population number for certain EU member states (-);

$L_{WWTP}$ = the proportion of a specific river network's length (m);

$L_{Total}$ = the total river network length in the country (m).

# 5 CHARACTERIZATION OF MICROPLASTIC PARTICLES

Current microplastic fate models typically assume microplastic particles to be spherical and then explore the impact of particle size and density on their distribution in freshwater systems. This approach is suboptimal to accurately capture the actual distribution of microplastics in rivers. For instance, the movement of fiber particles in water significantly differs from that of spherical microplastics, and since fibers represent a relatively important source of microplastics, treating all MP particles as spherical can lead to considerable uncertainty. An important difference between our model and existing freshwater microplastic transport models is that we assign specific size, density, and shape factors to each category of microplastics. This allows us to simulate their distribution in aquatic systems and sediment layers more precisely. Another advantage of our approach is the ability to individually compare our model's results with observed data on particular types of microplastics in rivers or lakes. For instance, we can compare the observed abundance of fibers or tyre wear particles (TWP) at specific locations in rivers. Furthermore, by aggregating the abundance of the seven most relevant sources of microplastics, we can obtain a comprehensive understanding of their overall distribution.

Following the outlined approach, our final report will contain seven subsections, each dedicated to describing the parameter settings for a specific type of microplastic. In this first version, we focus on the parameters for car tyre wear particles (TWP). Currently, we have set size bins specifically for tyre wear particles based on their typical particle size distribution observed in aquatic environments. For other types of microplastic sources, size bins will be defined according to their common size distributions in riverine system, rather than assigning a uniform classification to all particles. Additionally, for tyre wear particles, concentrations in various environmental compartments are calculated based on the mass of the particles. In subsequent studies, we plan to first quantify microfibers by number, and then convert these counts into mass to better integrate and compare findings across studies.

## 5.1 Tyre wear particles

For the parameter settings of tyre wear particles, our description will encompass three key aspects: size, shape, and density. Tyre wear particles are generated from the abrasion of vehicle tyres against road surfaces. They vary widely in size, typically ranging from a few nanometers to several hundred micrometers. Although models often assume these particles are spherical, they are more accurately described as ellipsoidal in shape. Furthermore, the density of these particles generally exceeds that of water, which influences their sedimentation and distribution in aquatic environments.

**(1) Size**

Figure **5** (Wagner et al., 2018) illustrates that the size distribution of TWP ranges from a few nanometers to several hundred micrometers. In a study conducted by Kreider et al. (2010), different types of tyres were tested on an asphalt road simulator. They found that the size distribution of the collected TWP ranged between 5.0 µm and 220 µm, with the greatest abundance occurring at 70–80 µm. Similar observations were made by Smolders and Degryse (2002), who found roadside TWP with a mean diameter of 65 µm for passenger vehicles and 80 µm for trucks.

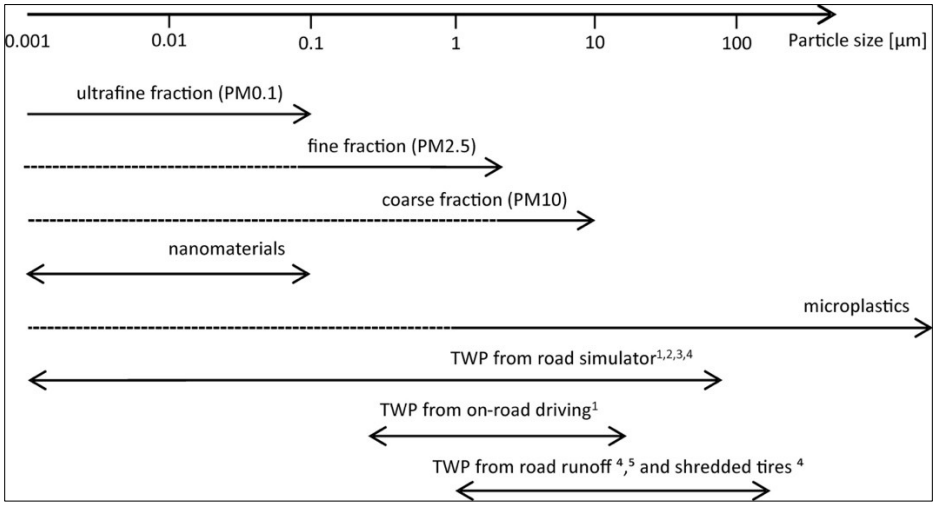


*Figure 4. Particle size ranges and obtained TWP size distributions. 1 (Kwak et al., 2013); 2 (Dahl et al., 2006); 3 (Gustafsson et al., 2008); 4 (Kreider et al., 2010); 5 (Wang et al., 2017). Derived from Wagner et al., 2018*

In our model, we use the size distribution results for TWP obtained by Kreider et al. (2010). This choice is based on the fact that their findings align closely with other empirical data and fall between the maximum and minimum values reported in other studies, as illustrated in Figure **6**. In this figure, the solid black line represents the findings from Kreider et al. (2010), while the light gray lines indicate the range of results from other studies, specifically the extreme scenarios of maximum and minimum values (Charters et al. 2015). Table **4** indicates the fraction of particles in each size bin based on the findings of Kreider et al. (2010). These fractions represent the mass percentages of particles that fall within each specified size range. We have defined five size classes with upper limits up to 250 µm to categorize TWP emissions.

| | *Particle Size Range (µm)* | | | | |
|---|---|---|---|---|---|
| *Mean particle size (µm)* | *<10 (5)* | *10-50 (30)* | *50-100 (75)* | *100-150 (125)* | *150-250 (200)* |
| | *Percent of particles (%)* | | | | |
| *110* | ***0.06%*** | ***10.84%*** | ***38.00%*** | ***32.00%*** | ***19.10%*** |

*Table 4. Size distribution of TWP used in the present model (base on Kreider et al., 2010)*

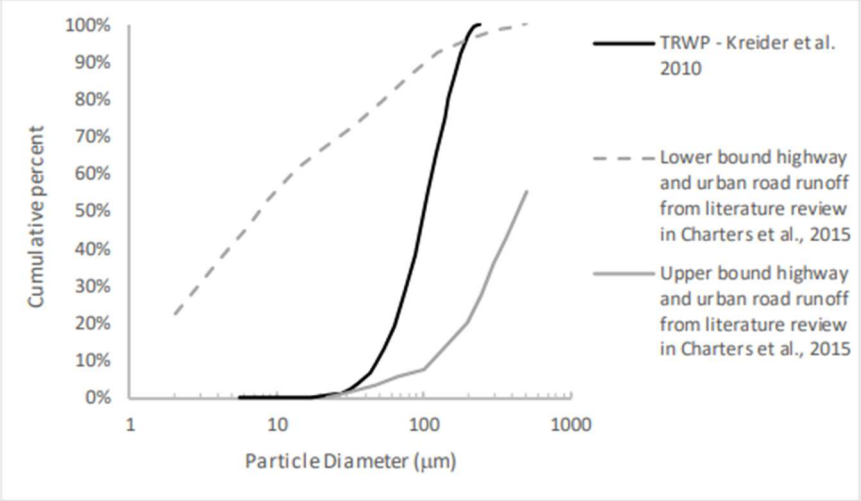


*Figure 6. Particle size distribution of TRWP from Kreider et al. (2010) with lower and upper bounds of urban road and highway runoff distributions summarized in Charters et al. (2015).*

### (2) Shape

Table **5** compiles the different morphological characteristics of Tyre Wear Particles (TWP) as observed in empirical studies under various sampling conditions. Figure **7**, based on the work of Parker et al. (2018), categorizes TWP into five types: sausage-like or tube-shaped particles (Type 1), spherical particles with a mean diameter of about 2.5 µm (Type 2), micron-sized debris with irregular morphologies (Type 3), and tiny spherical clusters of particles with diameters smaller than 50 nm (Type 4 and Type 5). Type 1 represents the original shape of TWP without secondary wear processes, which is frequently reported in studies. Type 2 is formed through the breaking down and surface smoothing of Type 1 during secondary wear processes. Type 3 with a diameter larger than 2.5 µm is derived from severe wear situations, such as cornering or braking. Type 4 and Type 5 have complex size distributions, and can form aggregates or adhere to larger particles.

| ***Sampling conditions*** | ***Morphology*** | ***Reference*** |
|---|---|---|
| *Road runoff, road simulator, shredded tyres* | ***Elongated, circularity 0.8, aspect ratio 0.64*** | *(Kreider et al., 2010)* |
| *Road simulator* | *Jagged, droplets, granules* | *(Gustafsson et al., 2008)* |
| *Road simulator, road runoff* | *Warped, porous* | *(Camatini et al., 2001)* |
| *Road runoff* | *Irregular* | *(Wang et al., 2017b)* |
| *Road simulator* | *Near spherical, elongated* | *(Dahl et al., 2006)* |

*Table 5. Morphologies of tyre materials obtained under various sampling conditions.*

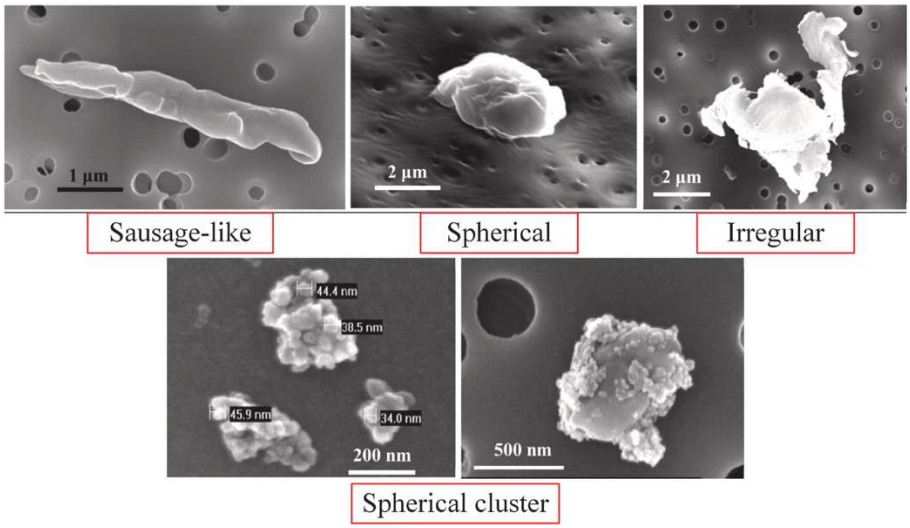


*Figure 7. SEM images of the five TWP types (Park et al., 2018).*

In summary, most previous research has observed that TWP are predominantly spherical or rod-shaped, similar to slender "sausages" (Kwak et al., 2014; Panko et al., 2018). Based on the observed shapes of TWP, we assume in our model that TWP particles are ellipsoidal. For these ellipsoidal particles, we define three dimensions: a as the intermediate dimension of the particle (m), b as the long dimension of the particle (m), and c as the short dimension of the particle (m). This approach allows for a more realistic representation of TWP shapes compared to assuming all particles are spherical. Additionally, we incorporate the Corey shape factor ($\psi$), which is a dimensionless number used to describe the deviation of a particle from a perfect sphere. This factor is particularly relevant for irregularly shaped particles like TWP. The Corey shape factor is defined in Equation 9.

$$\psi = \frac{c}{\sqrt{ab}} \qquad Equation\ 9$$

Following the cumulative density function for TWP proposed by Kreider et al. (2010) and referring to the parameter settings in the model by Unice et al. (2019), we will assume that the short axis and intermediate dimensions of the TWP are equal in length. When a particle's short (c) and intermediate (a) dimensions are considered to be the same, the shape factor can be expressed in terms of the aspect ratio, AR=w/l, with width, w=c=a, and length, l=b. Under these assumptions, the shape factor simplifies to a function of the aspect ratio.

$$\psi = \sqrt{w/l} = \sqrt{A_R} \qquad Equation\ 10$$

Therefore, using the mode value of the aspect ratio (width to length) of 0.64, as proposed by Kreider et al. (2010) (See Table 2), and using this value in Equation 10, we can calculate the corresponding Corey shape factor. With an aspect ratio of 0.64, the Corey shape factor is determined to be 0.80 (CSF=0.80).

**(3) Density**

Table **6** presents the result of literature review on the density distribution of Tyre Wear Particles (TWP) and Tyre and Road Wear Particles (TRWP) in real-world conditions, highlighting the wide variability in their densities. Observations range from a density of around 1.1 for pure tyre tread as measured by Rhodes et al. (2012), to as high as 2.4 in studies by Lavin (2003) and Li et al. (2016).

In the model parameters set by Unice et al. (2019), the density range for TRWP is specified as 0.94-2.4. They also noted that the probability of TRWP being less dense than water is low. Therefore, in our model parameter settings, we have chosen a density range of 1.1-2.4, with a central estimate of 1.8.

| *Literature review* | *Density range (g/cm3)* |
|---|---|
| *Jung and Choi, 2022* | *1.2 - 1.7* |
| *Klöckner et al., 2019* | *1.9* |
| *Sommer et al., 2018* | *1.26* |
| *Rhodes et al., 2012* | *1.13 - 1.16* |
| *Kayhanian et al., 2012* | *1.5 - 2.2* |
| *Rødland et al., 2023* | *1.2 - 2.3* |
| *Dannis, 1974* | *1.18* |
| *Sansalone and Tribouillard, 1999* | *1.5 - 1.7* |
| *Lavin, 2003; Li et al. 2016* | *2.4* |
| *Unice et al., 2019* | *0.94 - 2.4 (1.8)* |
| ***Our study*** | ***1.1-2.4 (1.8)*** |

*Table 6. Density distribution of TWP in literatures.*

**(4) Summary**

In summary, our model classifies Tyre Wear Particles (TWP) into five size categories and three density categories, with a uniform shape factor of 0.8. Consequently, we anticipate modelling a total of 15 different emission scenarios.

| *Our study* | *Diameter (μm)* | *Density (g/cm3)* | *Shape factor* |
|---|---|---|---|
| *Parameterization* | *5; 30; 75; 125; 200* | *1.1; 1.8; 2.4* | *0.8* |

*Table 7. Parameterization for TWP in our study.*

# 6 FATE PROCESSES

Once microplastics enter the aquatic environment, they undergo a series of fate processes (Figure **8**). The black arrows represent processes incorporated in the ePLAS model (Section **6.1-6.6**), while the white arrows indicate processes will be added in later stage (Section **6.7-6.8**). Overall, from the perspective of horizontal transport, microplastics are transported between the water layers of two river nodes via advection, and between the bed load layers via bed load transport. Internally within compartments, microplastics can undergo sedimentation and resuspension processes within both the water and sediment layers. Besides, microplastics undergo heteroaggregation with suspended particulate matter, which is another newly added and significant fate process in the updated model. In addition to the processes represented by the black arrows as described above, the white arrows indicating bioturbation also represent important exchange processes among different environmental compartments. These will be incorporated and updated in the model's technical report in a later stage.

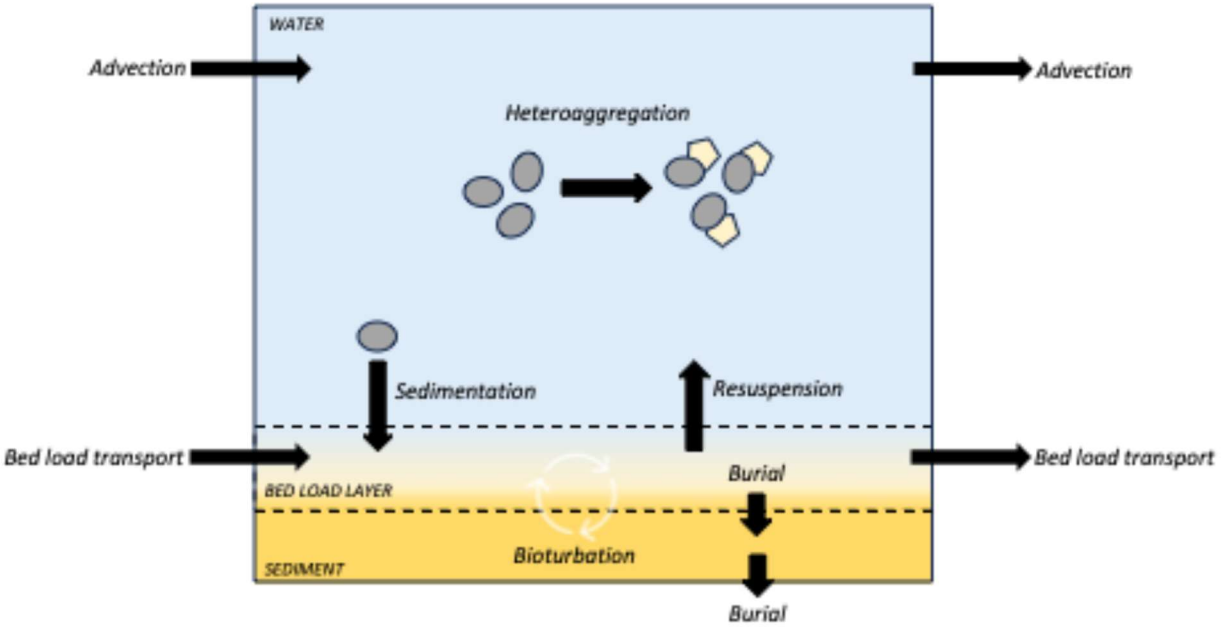


*Figure 8. Fate processes for microplastic in the riverine system. (Black arrows represent processes incorporated in ePLAS model, while the white arrows indicate processes will be added in later stage)*

## 6.1 Advection with water

Advection with water describes the longitudinal mass transfer of particles carried along by the flow of water. The model disregards diffusive transport of microplastics in the water phase because advection typically dominates diffusion in dynamic river environments, especially for large and lightweight particles (Mennekes et al., 2023). It is thus assumed that all particles in the water column are homogeneously distributed. Advection is described by Equation **11** (Domercq et al., 2022):

$$k_{flow} = \overline{v_{flowRiver}} \times \frac{A_{comp}}{Q_{comp}} \qquad Equation\ 11$$

where,

$k_{flow}$ = the advection rate ($s^{-1}$);

$\overline{v_{flowRiver}}$ = the average flow velocity of water (m/s) (Table **1**);

$A_{comp}$ = the cross-sectional area of the compartment ($m^2$);

$Q_{comp}$ = the volume of the moving water ($m^3$).

## 6.2 Sedimentation

Sedimentation refers to the transport of microplastic particles from the water column to the sediment due to gravitational forces. This process is influenced by the specific characteristics of both the freshwater environment and the microplastic particles themselves. In rivers, sedimentation typically occurs in areas with lower flow velocities, such as confluences of multiple streams and bends in the river, where the reduced kinetic energy allows particles to settle (Wang et al., 2020; Zhang et al., 2021). Conversely, in lake environments, where flow velocities are generally lower, a significant proportion of microplastics tends to sediment into the lakebed (Horton and Dixon, 2018; Waldschläger et al., 2020). The rate of sedimentation is also affected by the density, shape, and size of the microplastic particles, as indicated by empirical formulas that relate settling velocity to these physical characteristics (Dioguardi et al., 2018; Van Melkebeke et al., 2020).

The sedimentation process for microplastic can be described by Equation **12** and Equation **13** (Turton and Clark, 1987):

$$v_{set}^{MP} = \left(\left(\frac{\rho_{MP}}{\rho_w} - 1\right) \cdot g \cdot \mu_k\right)^{\frac{1}{3}} \cdot \left(\left(\frac{4}{3} \cdot \frac{{d_*^{MP}}^2}{A}\right)^{-1} + \left(\frac{\sqrt{d_*^{MP}}}{\alpha}\right)^{-1}\right)^{-1} \qquad Equation\ 12$$

and $d_*$ the non-dimensionalized particle size, computed as:

$$d_*^{MP} = d_{MP}\left(\left(\frac{\rho_{MP}}{\rho_w} - 1\right) \cdot \frac{g}{\mu_k}\right)^{\frac{1}{3}} \qquad Equation\ 13$$

where,

$v_{set}^{MP}$ = the settling velocity for an individual microplastic particle (m/s);

$\rho_{MP}$ = the density of microplastic ($kg/m^3$) (user input; default value 1.8 $kg/m^3$);

$\rho_w$ = the density of water ($kg/m^3$) (user input; default value 0.9996 $kg/m^3$);

$g$ = the gravitational acceleration ($m/s^2$), with a standard value of 9.81 $m/s^2$;

$d_{MP}$ = the equivalent particle diameter (m) (user input; see Table **7**);

$d_*^{MP}$ = the dimensionless diameter (-);

A = a constant depending on the shape factor, with a standard value of 32 (-);

$\alpha$ = a constant depending on the shape factor, with a standard value of 0.86 (-);

$\mu_k$ = the kinematic viscosity ($m^2/s$).

## 6.3 Resuspension

Resuspension (or re-entrainment) refers to the re-entry of particles from the sediment back into the water column due to disturbances such as strong water currents or biological activity (Domercq et al., 2022). While different equations are being used for modelling resuspension, the definition of the process remains consistent: resuspension occurs only when the shear stress exceeds a critical threshold. This critical shear stress is the point at which the forces acting on the particles in the sediment are sufficient to overcome the forces keeping them in place, leading to their mobilization back into the water column. Environmental conditions such as heavy

rain, floods, and boat traffic in canals can also impact resuspension rates. For instance, higher shear forces and increased flow velocities during such events can lead to the resuspension of microplastics that have previously sedimented. (Kooi et al., 2018; Wang et al., 2020).

Moreover, it is important to consider the process of turbulent entrainment, which explains why particles heavier than water can be lifted back into suspension. This is distinct from resuspension (which refers to erosion). In depth-averaged models like ePLAS, this phenomenon is traditionally addressed by applying a correction factor to the deposition flux, following the method proposed by Ray Krone (1962, 1964). While this correction has not yet been implemented in our model, it represents a critical future enhancement to more accurately simulate the dynamics of microplastic transport and sedimentation.

Resuspension is modelled by Equations **14-19** (Van Rijn, 1993; Chanson, 2004; Besseling et al., 2016; Unice et al., 2019; Wu, 2007; Waldschlager and Schuttrumpf, 2019).

**Shear stress:**

$$\tau_0 = \rho_w \cdot g \cdot \left(\frac{\overline{v_{\text{flowRiver}}}}{C_h}\right)^2 \qquad Equation\ 14$$

**The critical shear stress:**

$$\tau_c = \phi_c \cdot (\rho_{MP} - \rho_w) \cdot g \cdot d_{MP} \qquad Equation\ 15$$

$$\phi_c = 0.5588\phi_{c,sed} \cdot \left(\frac{d_{MP}}{d_{50}}\right)^{-0.503} \qquad Equation\ 16$$

$$\phi_{c,sed} = \begin{cases} 0.126{d_*}^{-0.44} & d_* < 1.5 \\ 0.131{d_*}^{-0.55} & 1.5 < d_* < 10 \\ 0.0685{d_*}^{-0.27} & 10 \le d_* \le 20 \\ 0.0173{d_*}^{0.19} & 20 \le d_* \le 40 \\ 0.0115{d_*}^{0.30} & 40 \le d_* \le 150 \\ 0.052 & d_* \ge 150 \end{cases} \qquad Equation\ 17$$

$$d_* = d_{50} \cdot \left(\frac{\left(\frac{\rho_{sed}}{\rho_w}\right) g}{{\mu_k}^2}\right)^{\frac{1}{3}} \qquad Equation\ 18$$

When $\tau_c > \tau_0$, resuspension is modelled as a first order process, as suggested by Partheniades (1965) (Van Kessel et al., 2011; De Klein et al., 2016; Besseling et al., 2017). R is based on the ratio between the shear stress and critical shear stress, multiplied with the resuspension parameter $R_{sed}$ (kg/m$^2$day):

$$R = f_{MP} \cdot R_{sed} \cdot \left(\frac{\tau}{\tau_c} - 1\right) \qquad Equation\ 19$$

where,

$\tau_0$ = the shear stress (Pa or kg/m*s$^2$);

$\rho_w$ = the density of water (kg/m$^3$) (user input; default value 0.9996 kg/m$^3$);

$\rho_{sed}$ = the density of sediment (kg/m$^3$) (user input; default value 2.5 kg/m$^3$);

$g$ = the gravitational acceleration (m/s$^2$), with a standard value of 9.81 m/s$^2$;

$\overline{v_{flowRiver}}$ = the average flow velocity (m/s) (Table 1);

$C_h$ = the Chézy coefficient ($m^{0.5}/s$) (user input; default value 40 $m^{0.5}/s$);

$\tau_c$ = the critical shear stress (Pa or kg/m*$s^2$);

$\Phi_c$ = the critical Shields number (-);

$\Phi_{c,\,sed}$ = the critical Shields number for sediment (-);

$d_{MP}$ = the equivalent particle diameter of MP (m);

$d_*$ = the dimensionless diameter (-);

$d_{50}$ = the median sediment diameter (m) (user input; default value 0.001m);

$\mu_k$ = the kinematic viscosity ($m^2/s$);

$R$ = the ratio between the shear stress and critical shear stress (kg/$m^2$*day);

$f_{MP}$ = the mass fraction of plastic in the sediment (%);

$R_{sed}$ = the resuspension parameter (kg/$m^2$*day) (user input; default value 0.0001 kg/$m^2$*day).

### 6.4 Heteroaggregation

Heterogeneous aggregation (or heteroaggregation) refers to the process of aggregation between plastic particles and natural suspended particulate matter (SPM). The Full Multi model (Domercq et al., 2022) and the NanoDUFLOW model (Besseling et al., 2016) describe heteroaggregation as a pseudo-first-order process according to classic colloid theory. The rate constant of this process depends on the collision frequency between the two types of particles, the concentration of SPM in the system, and the attachment efficiency of heteroaggregation (*α_het_agg*). The latter parameter represents the probability of forming a heteroaggregate upon collision. *α_het_agg* reflects the degree of interaction between plastic particles and SPM, and it is influenced by the surface properties of the colliding particles and the chemical environment of the water.

It is important to note that in the current version of the ePLAS model, heteroaggregation is treated as a dissipation process. This means that once microplastics get heteroaggregated, they are considered removed from the water column for further tracking within the model framework. However, we plan to track the concentrations of these heteroaggregated particles across different environmental compartments in future versions of the model, but this feature has not yet been implemented.

Heteroaggregation is described by Equations **20**-**21**:

Heteroaggregation rate:

$$k_{hetAgg} = \alpha_{\text{het-agg}} \times k_{\text{coll}} \times N_{\text{SPM}} \qquad Equation\ 20$$

Collision frequency:

$$k_{\text{coll}} = \frac{2k_b T_w}{3\mu_w}\frac{(d_{MP}+d_{SPM})^2}{d_{MP}\cdot d_{SPM}} + \frac{1}{6}G(d_{MP}+d_{SPM})^3 + \frac{\pi}{4}(d_{MP}+d_{SPM})^2\left|v_{set}^{MP} - v_{set}^{SPM}\right|$$

*Equation* 21

where,

$k_{hetAgg}$ = the heteroaggregation rate ($s^{-1}$);

$a_{het\text{-}agg}$ = the heteroaggregation attachment efficiency (user input; default value 0.01);

$N_{SPM}$ = the number concentration of suspended solids (particles/$m^3$);

$k_{coll}$ = the collision rate constant ($m^3$/s);

$T_w$ = the local water temperature (K) (user input; default value 285 K);

$k_b$ = the Boltzmann constant (J/K), with a standard value of 1.38 x $10^{-23}$m/$s^2$;

$d_{MP}$ = the equivalent particle diameter of MP (m);

$d_{SPM}$ = the equivalent particle diameter of suspended solids (m) (Table **8**);

$\mu_w$ = the dynamic viscosity of water at 11.4°C (kg/m*s), (user input; 0.001255 kg/m*s);

$v^{MP}_{set}$ = the settling velocity of microplastics (m/s) (Equation **12**);

$v^{SPM}_{set}$ = the settling velocity of suspended solids (m/s) (Equation **12**).

***Suspended particulate matter***

SPM is assumed to be present as a distribution of (aggregated) primary particles (Table **7**). The particles are assumed to follow a lognormal particle size distribution, which is divided into 5 size classes for the model calculations. In addition, we assume that the settling velocity of SPM particles follows the same equation as microplastics (Equation **12** and Equation **13**).

| *Parameter* | *Symbol* | *Value* | *Unit* | *Reference* |
|---|---|---|---|---|
| *Parameters of lognormal size distribution* | $mode_{SPM}$ | *5* | *µm* | *Praetorius et al., 2012* |
| | $\mu_{ln.SPM}$ | *9.9* | *µm* | *Praetorius et al., 2012* |
| | $\sigma_{ln,SPM}$ | *0.59* | *µm* | *Praetorius et al., 2012* |
| *Average mass concentration of SPM* | $C_{SPM}$ | *30* | *mg/L* | *Dormercq et al., 2022* |
| *Number of SPM size classes in the model* | $N_{SPM}$ | *5* | *-* | *-* |
| *Diameter of SPM in size classes* | $d_{SPM,j}$ | *[0.5,1.5,5.0,15,50]* | *µm* | *Besseling et al., 2016* |
| *Radius of SPM in size class* | $R_{SPM,j}$ | $d_{SPM,j}$ / 2 | *µm* | *-* |

| | | | | |
|---|---|---|---|---|
| *Average SPM density* | $\rho_{SPM}$ | *2.12* | *kg/m3* | *Besseling et al., 2016* |

*Table 8. Parameterization for SPM in our study*

## 6.5 Sediment transport

The sedimentation dynamics in aquatic environments is characterized by a complex interplay between vertical accumulation and horizontal transport processes. Typically, sediments are stratified into two distinct layers: the upper active layer (bed load layer) and the lower inactive layer (sediment layer). The upper active layer is characterized by looser sediments that are susceptible to disturbances, such as water currents, which facilitate the horizontal bed load transfer. This process involves the movement of sediment particles along the bottom of the water body, driven by the flow of the water. Particles within this layer can be resuspended back into the water column, contributing to the continuous redistribution of sediments and associated microplastic particles across the aquatic floor. We adopt the concept of an active sediment layer including horizontal bed load transfer (Praetorius et al., 2012). The sediment transport process is described by Equations **22**-**23**.

$$k_{se\ \ transfer,n} = \frac{v_{sed\_trans}}{m_{sed}} \qquad Equation\ 22$$

$$m_{sed} = (1 - \phi_{sed}) * \rho_{sed} * V_{sed} \qquad Equation\ 23$$

where,

$k_{sedtransfer,n}$ = the sediment transfer rate ($s^{-1}$);

$v_{sed\_trans}$ = the velocity of sediment transfer (kg/s) (user input; default value 3.0 kg/s);

$m_{sed}$ = the mass of sediment of the river sediment (kg);

$\Phi_{sed}$ = the porosity of the sediment (-);

$\rho_{sed}$ = the density of sediment ($kg/m^3$) (user input; default value 2.5 $kg/m^3$);

$V_{sed}$ = the volume of the sediment ($m^3$).

## 6.6 Burial

As sediments accumulate, they transition from the dynamic, disturbance-prone upper active layer to the denser, more stable lower inactive layer, also known as the stagnant sediment layer. The main function of this layer is to serve as an intermediary zone where burial predominantly occurs sediment deposition exceeds the amount resuspended, leading to a gradual accumulation of sediment and the encapsulation of microplastic particles over time (Besseling et al., 2016). Once microplastic particles migrate into this stagnant layer, typically the first 10 cm of sediment, they become buried and are no longer subject to resuspension processes under normal conditions.

This burial process is effectively modeled as a first-order kinetic process, where the rate of burial at the sediment surface is generally proportional to the concentration of microplastic in the surface sediments. This makes the buried microplastic particles a slow dissipation mechanism in the sedimentary environment (Koelmans et al., 2009). Importantly, the stagnant sediment layer acts as both an import zone for burial from the bed load layer and as an export zone for deeper sediment layers. Under steady-state conditions, the concentration of microplastics in this stagnant sediment layer is expected to equal the concentration in the bed

load layer. However, this equilibrium can change with the inclusion of bioturbation and under dynamic environmental conditions. Bioturbation, which typically affects between the bed load layer and the first 10 cm of sediment, will be considered in future stages of the model to refine our understanding of microplastic dynamics within this sediment layer.

An average burial velocity of 0.25 cm/year was used, which is the value of a review to bioturbation in the marine environment for Elbe River Basin (Kossel et al., 2024; Deek et al., 2013). An average mixing depth of 10 cm was used, which was found to be a robust worldwide average (Boudreau, 1994). This results in a burial rate of $7.93\times10^{-10}$ $s^{-1}$. The burial process can be described by equation **24**.

$$k_{bur} = 7.93 \times 10^{-10} s^{-1} \qquad Equation\ 24$$

where,

$k_{bur}$ = the burial rate of microplastics ($s^{-1}$).

## 6.7 Bioturbation

Bioturbation significantly yet complexly impacts the transport and deposition of microplastics in sedimentary environments. Bioturbation refers to disturbances in sediments caused by biological activities, which can alter the physical states of both microplastics and natural sediments (Waldschlager et al., 2022). For instance, the burrowing and foraging behaviors of benthic organisms can lead to the vertical mixing and redistribution of microplastics within sediment layers. The interaction between biological activities and microplastic transport is complicated. Bioturbation can result in microplastics being embedded deeper into sediment layers or re-entering the water column.

However, existing literature indicates substantial variability in the impacts of different species and their ecological functions on these processes (Cozzoli et al., 2019). This variability arises from differences in biological behavior, sediment characteristics, and environmental conditions. Therefore, further research is necessary before incorporating these as diffuse sources into each river segment of the ePLAS model to enhance its application effectively.

## 6.8 Mass balance equations

Upon establishing river environmental parameters, microplastic particle settings, and their fate processes, it is crucial to formulate mass balance equations for each river stretch. We provide a schematic illustration at the start node, which include the water layer, the bed load layer and the stagnant sediment layer.

### 6.8.1 Mass balance equation for free TWP particles (For Box = 1)

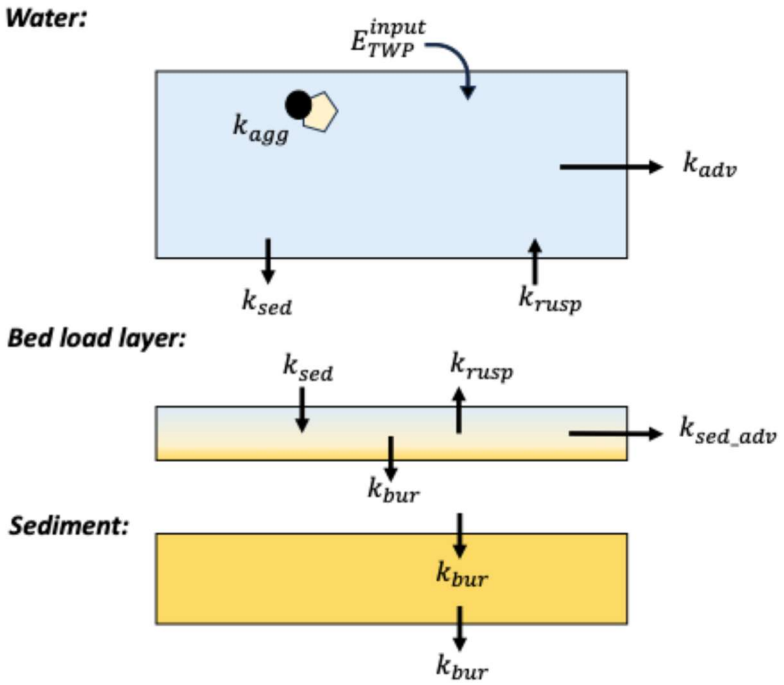


*Figure 9. A schematic diagram of different environmental compartments including fate processes (using the START point as an example). Note: the ETWP referred to in the diagram represents the point source or diffuse source emissions discussed in the previous chapter.*

The current version adopts a strategy of calculating steady-state mass of microplastics (tyre wear particles in this version) in the water and sediment layers, thereby making the left-hand terms of Equations **28** and **29**, namely the particle change rate, equal to zero.

***Water layer:***

$$\frac{dM_w}{dt} = E_{TWP}^{input} + M_{bed} \cdot k_{rusp} - \left(k_{agg} + k_{sed} + k_{adv}\right) \cdot M_w \qquad Equation\ 25$$

***Bed load layer:***

$$\frac{dM_{bed}}{dt} = M_w \cdot k_{sed} - \left(k_{rusp} + k_{bur} + k_{sed\_adv}\right) \cdot M_{bed} \qquad Equation\ 26$$

***Sediment layer:***

$$\frac{dM_{sed}}{dt} = M_{bed} \cdot k_{bur} - M_{sed} \cdot k_{bur} \qquad Equation\ 27$$

where,

$dM/dt$ = the rate of change of tyre wear particle mass in different compartments(kg/s);

$E^{input}_{TWP}$ = the input emissions from point and diffused sources of tyre wear particles (kg/s), as discussed in Section **4.4.2** (Equation **7** and **8**);

$k_{rusp}$ = the resuspension rate of tyre wear particles ($s^{-1}$);

$k_{agg}$ = the heteroaggregation rate of tyre wear particles ($s^{-1}$);

$k_{sed}$ = the sedimentation rate of tyre wear particles ($s^{-1}$);

$k_{adv}$ = the advection rate of tyre wear particles ($s^{-1}$);

$k_{sed\_adv}$ = the sediment transfer rate of tyre wear particles ($s^{-1}$);

$M_w$ = the mass of tyre wear particles in water layer (kg);

$M_{bed}$ = the mass of tyre wear particles in bed load layer (kg);

$M_{sed}$ = the mass of tyre wear particles in sediment layer (kg).

### 6.8.2 Solving the mass balance equation under steady-state condition for the first box

From Equation **26**, the mass of microplastic particles in the sediment layer can be derived, as shown in Equation **28**:

$$M_{bed} = \frac{M_w \cdot k_{sed}}{k_{rusp} + k_{bur} + k_{sed\_adv}} \qquad Equation\ 28$$

where,

$k_{rusp}$ = the resuspension rate of tyre wear particles ($s^{-1}$);

$k_{bur}$ = the burial rate of tyre wear particles ($s^{-1}$);

$k_{sed}$ = the sedimentation rate of tyre wear particles ($s^{-1}$);

$k_{sed\_adv}$ = the sediment transfer rate of tyre wear particles ($s^{-1}$);

$M_w$ = the mass of tyre wear particles in water layer(kg);

$M_{bed}$ = the mass of tyre wear particles in bed load layer (kg).

Substituting Equation **28** back into Equation **25** yields Equation **29**, which represents the mass of microplastics in the water layer.

$$M_w = \frac{E_{TWP}^{input} + k_{rusp} \cdot \frac{M_w \cdot k_{sed}}{k_{rusp} + k_{bur} + k_{sed\_adv}}}{k_{agg} + k_{sed} + k_{adv}} \qquad Equation\ 29$$

where,

$E^{input}_{TWP}$ = the input emissions from point and diffused sources of tyre wear particles (kg/s), as discussed in Section **4.4.2** (Equation **7** and **8**);

$k_{rusp}$ = the resuspension rate of tyre wear particles ($s^{-1}$);

$k_{agg}$ = the heteroaggregation rate of tyre wear particles ($s^{-1}$);

$k_{sed}$ = the sedimentation rate of tyre wear particles ($s^{-1}$);

$k_{adv}$ = the advection rate of tyre wear particles ($s^{-1}$);

$k_{sed\_adv}$ = the sediment transfer rate of tyre wear particles ($s^{-1}$);

$M_w$ = the mass of tyre wear particles in water layer (kg);

$M_{bed}$ = the mass of tyre wear particles in bed load layer (kg);

$M_{sed}$ = the mass of tyre wear particles in sediment layer (kg).

By combining Equations **28** and **29**, Equation **30** and **31** can be derived, which represent the expressions for the mass of microplastics in the water layer and sediment layer, respectively, under long-term steady-state conditions (the *START* point)

***Water layer:***

$$M_w = \frac{E_{TWP}^{input}}{k_{agg} + k_{sed} + k_{adv} - \frac{k_{rusp} \cdot k_{sed}}{k_{rusp} + k_{bur} + k_{sed\_adv}}} \quad Equation\ 30$$

***Bed load layer:***

$$M_{bed} = \frac{k_{sed} \cdot E_{TWP}^{input}}{(k_{agg} + k_{sed} + k_{adv}) \cdot (k_{rusp} + k_{bur} + k_{sed_{adv}}) - k_{rusp} \cdot k_{sed}} \quad Equation\ 31$$

***Sediment layer:***

$$M_{sed} = M_{bed} \quad Equation\ 32$$

where,

$dM/dt$ = the rate of change of tyre wear particle mass in different compartments(kg/s);

$E^{input}_{TWP}$ = the input emissions from point and diffused sources of tyre wear particles (kg/s), as discussed in Section **4.4.2** (Equation **7** and **8**);

$k_{rusp}$ = the resuspension rate of tyre wear particles ($s^{-1}$);

$k_{agg}$ = the heteroaggregation rate of tyre wear particles ($s^{-1}$);

$k_{sed}$ = the sedimentation rate of tyre wear particles ($s^{-1}$);

$k_{adv}$ = the advection rate of tyre wear particles ($s^{-1}$);

$k_{sed\_adv}$ = the sediment transfer rate of tyre wear particles ($s^{-1}$);

$M_w$ = the mass of tyre wear particles in water layer (kg);

$M_{bed}$ = the mass of tyre wear particles in bed load layer (kg);

$M_{sed}$ = the mass of tyre wear particles in sediment layer (kg).

### 6.8.3 Solving the mass balance equation under steady state conditions for box = 2 to i

Equations **33** and **34** represent the long-term steady-state mass of microplastics in the water layer bed load transport layer and sediment layer, respectively, starting from the second node in the river network following the START node. It is important to note that, as these are mass conservation equations beginning from the second node, there will initially be inputs of water concentrations and sediment concentrations from the START node's upstream flowing into the current node.

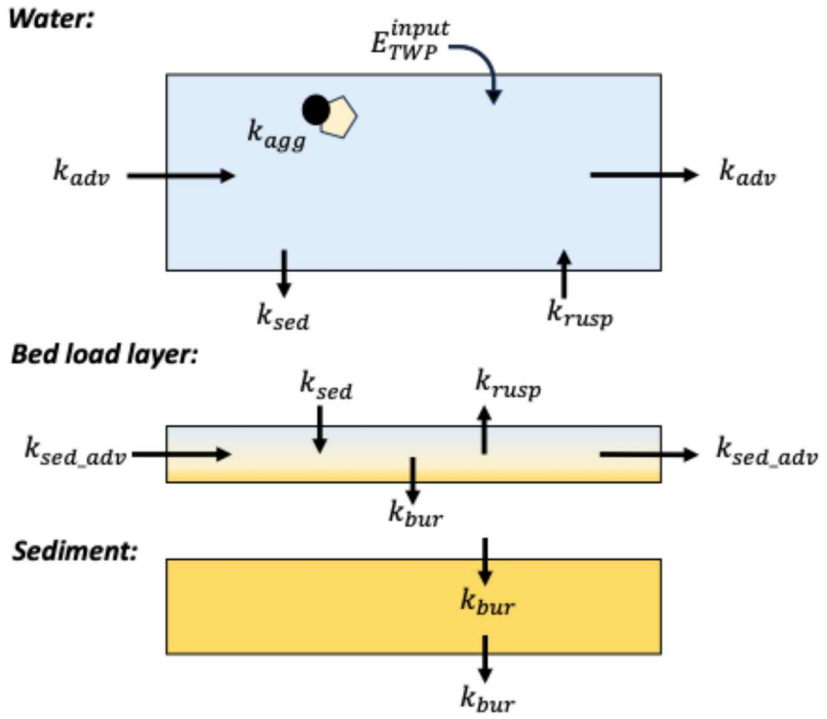


*Figure 10. A schematic diagram of different environmental compartments including fate processes (Starting at the second node after the START node). Note: the ETWP referred to in the diagram represents the point source or diffuse source emissions discussed in the previous chapter.*

***Water layer:***

$$M_w = \frac{E_{up\_w} + \frac{k_{rusp} \cdot E_{up\_sed}}{k_{rusp} + k_{bur} + k_{sed\_adv}} + E_{TWP}^{input}}{k_{agg} + k_{sed} + k_{adv} - \frac{k_{rusp} \cdot k_{sed}}{k_{rusp} + k_{bur} + k_{sed\_adv}}} \quad Equation\ 33$$

***Bed load layer:***

$$M_{sed} = \frac{E_{up_{sed}} + \left( \frac{E_{up\_w} + \frac{k_{rusp} \cdot E_{up\_sed}}{k_{rusp} + k_{bur} + k_{sed\_adv}} + E_{TWP}^{input}}{k_{agg} + k_{sed} + k_{adv} - \frac{k_{rusp} \cdot k_{sed}}{k_{rusp} + k_{bur} + k_{sed\_adv}}} \right) \cdot k_{sed}}{k_{rusp} + k_{bur} + k_{sed\_adv}} \quad Equation\ 34$$

***Sediment layer:***

$$M_{sed} = M_{bed} \cdot k_{bur} \quad Equation\ 35$$

where,

$E_{up\_w\_mass}$ = the mass for the water phase from the previous node, which is typically calculated by multiplying the mass concentration in the water phase at the previous node by the advective flow rate at that node (kg/s);

$E_{up\_w\_mass}[j] = N_{w\_mass}[j\text{-}1] * k_{adv}[j\text{-}1]$;

$E_{up\_sed\_mass}$ = the mass for the sediment phase from the previous node, which is typically

calculated by multiplying the mass concentration in the sediment phase at the previous node by the sediment transfer rate at that node (kg/s);

$E_{up\_sed\_mass}[j] = N_{sed\_mass}[j-1] * k_{sed\_adv}[j-1]$;

$E^{input}_{TWP}$ = the input emissions from point and diffused sources of tyre wear particles (kg/s), as discussed in Section **4.4.2** (Equation **7** and **8**);

$k_{rusp}$ = the resuspension rate of tyre wear particles ($s^{-1}$);

$k_{agg}$ = the heteroaggregation rate of tyre wear particles ($s^{-1}$);

$k_{sed}$ = the sedimentation rate of tyre wear particles ($s^{-1}$);

$k_{adv}$ = the advection rate of tyre wear particles ($s^{-1}$);

$k_{sed\_adv}$ = the sediment transfer rate of tyre wear particles ($s^{-1}$);

$M_w$ = the mass of tyre wear particles in water layer (kg);

$M_{bed}$ = the mass of tyre wear particles in bed load layer (kg);

$M_{sed}$ = the mass of tyre wear particles in sediment layer (kg).

## LITERATURE

Ali, S. S., Al-Tohamy, R., Sun, J., Wu, J., & Huang, M. (2018). The role of gut symbionts from termites: A unique hidden player from yeasts. Acta Microbiol Sin, 58(6), 1004-1015. https://doi.org/10.13343/j.cnki.wsxb.201706

Ali, S. S., Al-Tohamy, R., Manni, A., Luz, F. C., Elsamahy, T., & Sun, J. (2019). Enhanced digestion of bio-pretreated sawdust using a novel bacterial consortium: Microbial community structure and methane-producing pathways. Fuel, 254, 115604. https://doi.org/10.1016/j.fuel.2019.06.012

Ali, S. S., & Sun, J. (2019). Effective thermal pretreatment of water hyacinth (Eichhornia crassipes) for the enhancement of biomethanation: VIT® gene probe technology for microbial community analysis with special reference to methanogenic Archaea. Journal of Environmental Chemical Engineering, 7, 102853. https://doi.org/10.1016/j.jece.2018.102853

Andrady, A. L. (2011). Microplastics in the marine environment. Marine Pollution Bulletin, 62, 1596-1605. https://doi.org/10.1016/j.marpolbul.2011.05.030

Andrady, A. L. (2015). Degradation of plastics in the environment. In A. L. Andrady (Ed.), Plastics and Environmental Sustainability (pp. 1-15). John Wiley & Sons.

Andrady, A. L., Barnes, P. W., Bornman, J. F., Gouind, T., Madronich, S., White, C. C., Zepp, R. G., & Jansen, M. A. K. (2022). Oxidation and fragmentation of plastics in a changing environment; from UV-radiation to biological degradation. Science of the Total Environment, 851, 158022. https://doi.org/10.1016/j.scitotenv.2022.158022

Ani, E.-C., Wallis, S., Kraslawski, A., & Agachi, P. S. (2009). Development, calibration and evaluation of two mathematical models for pollutant transport in a small river. Environmental Modelling & Software, 24(10), 1139–1152.

Biffinger, J. C., Barlow, D. E., Pirlo, R. K., Babson, D. M., Fitzgerald, L. A., Zingarelli, S., Nadeau, L. J., Crookes-Goodson, W. J., & Russell, J. N. Jr. (2014). A direct quantitative agar-plate based assay for analysis of Pseudomonas protegens Pf-5 degradation of polyurethane films. International Biodeterioration & Biodegradation, 95, 311-319. https://doi.org/10.1016/j.ibiod.2014.09.005

Booth, A. M., Kubowicz, S., Beegle-Krause, C., Skancke, J., Nordam, T., Landsem, E., & Jahren, S. (2017). Microplastic in global and Norwegian marine environments: Distributions, degradation mechanisms and transport. SINTEF Ocean AS. (M-918/2017; p. 149).

Chamas, A., Moon, H., Zheng, J., Qiu, Y., Tabassum, T., Jang, J. H., ... & Suh, S. (2020). Degradation rates of plastics in the environment. ACS Sustainable Chemistry & Engineering, 8(9), 3494-3511.

Charters, F. J., Cochrane, T. A., & O'Sullivan, A. D. (2015). Particle size distribution variance in untreated urban runoff and its implication on treatment selection. Water Research, 85, 337-345.

Chubarenko, I., Efimova, I., Bagaeva, M., Bagaev, A., & Isachenko, I. (2020). On mechanical fragmentation of single-use plastics in the sea swash zone with different types of bottom sediments: Insights from laboratory experiments. Marine Pollution Bulletin, 150, 110726. https://doi.org/10.1016/j.marpolbul.2019.110726

Corcoran, P. L., Biesinger, M. C., & Grifi, M. (2009). Plastics and beaches: A degrading relationship. Marine Pollution Bulletin, 58, 80-84. https://doi.org/10.1016/j.marpolbul.2008.08.022

Cunningham, M., Ehlers, S., Dick, J., Sigwart, J., Linse, K., Dick, J., Kiriakoulakis, K. (2020). High abundances of microplastic pollution in deep-sea sediments: Evidence from Antarctica and the Southern Ocean. Environmental Science & Technology, 54(21). https://doi.org/10.1021/acs.est.0c03441

Da Costa, J. P., Nunes, A. R., Santos, P. S. M., Girão, A. V., Duarte, A. C., & Rocha-Santos, T. (2018). Degradation of polyethylene microplastics in seawater: Insights into the environmental degradation of polymers. Journal of Environmental Science and Health, Part A: Toxic/Hazardous Substances & Environmental Engineering, 53, 866-875.

Dahl, A., Gharibi, A., Swietlicki, E., Gudmundsson, A., Bohgard, M., Ljungman, A., Blomqvist, G., & Gustafsson, M. (2006). Traffic-generated emissions of ultrafine particles from pavement-tire interface. Atmospheric Environment, 40, 1314-1323. https://doi.org/10.1016/j.atmosenv.2005.10.029

Delre, A., Goudriaan, M., Morales, V. H., Vaksmaa, A., Ndhlovu, R. T., Baas, M., ... & Niemann, H. (2023). Plastic photodegradation under simulated marine conditions. Marine Pollution Bulletin, 187, 114544.

Dietrich, W. E. (1982). Settling Velocity of Natural Particles. Water Resources Research, 18(6), 1615-1626. https://doi.org/10.1029/WR018i006p01615

Dimassi, S. N., Hahladakis, J. N., Yahia, M. N. D., Ahmad, M. I., Sayadi, S., & Al-Ghouti, M. A. (2022). Degradation-fragmentation of marine plastic waste and their environmental implications: A critical review. Arabian Journal of Chemistry, 15(11), 104262. https://doi.org/10.1016/j.arabjc.2022.104262

Dioguardi, F., Mele, D., & Dellino, P. (2018). A new one-equation model of fluid drag for irregularly shaped particles valid over a wide range of Reynolds number. Journal of Geophysical Research: Solid Earth, 123(1), 144-156.

Dris, R., Imhof, H., Sanchez, W., et al. (2015). Beyond the ocean: Contamination of freshwater ecosystems with (micro-) plastic particles. Environmental Chemistry, 12, 539-550.

EEA (2015). UWWTD-WaterBase. Available from: http://www.eea.europa.eu/data-and-maps/data/waterbase-uwwtd-urban-waste-water-treatment-directive-4. European Environmental Agency. Latest update at 19 February 2015.

Enders, K., Lenz, R., Stedmon, C. A., & Nielsen, T. G. (2015). Abundance, size and polymer composition of marine microplastics ≥ 10 μm in the Atlantic Ocean and their modelled vertical distribution. Marine Pollution Bulletin, 100, 70-81. https://doi.org/10.1016/j.marpolbul.2015.09.027

Eriksen, M. et al. (2014). Plastic pollution in the world's oceans: More than 5 trillion plastic pieces weighing over 250,000 tons afloat at sea. PLoS ONE, 9, e111913.

Faure, F., Demars, C., Wieser, O., et al. (2015). Plastic pollution in Swiss surface waters: Nature and concentrations, interaction with pollutants. Environmental Chemistry, 12, 582-591.

Fragão, J., Bessa, F., Otero, V., Barbosa, A., Sobral, P., Waluda, C., Guímaro, H., Xavier, J. (2021). Microplastics and other anthropogenic particles in Antarctica: Using penguins as biological samplers. Science of the Total Environment, 788, 147698. https://doi.org/10.1016/j.scitotenv.2021.147698

Gijsman, P., Meijers, G., & Vitarelli, G. (1999). Comparison of the UV-degradation chemistry of polypropylene, polyethylene, polyamide 6, and polybutylene terephthalate. Polymer Degradation and Stability, 65, 433-441. https://doi.org/10.1016/S0141-3910(99)00033-6

Gustafsson, M., Blomqvist, G., Gudmundsson, A., Dahl, A., Swietlicki, E., Bohgard, M., Lindbom, J., & Ljungman, A. (2008). Properties and toxicological effects of particles from the interaction between tyres, road pavement and winter traction material. Science of the Total Environment, 393, 226-240. https://doi.org/10.1016/j.scitotenv.2007.12.030

Gewert, B., Plassmann, M. M., & MacLeod, M. (2015). Pathways for degradation of plastic polymers floating in the marine environment. Environmental Science & Process Impacts, 17(9), 1513-1521. https://doi.org/10.1039/C5EM00207A

Horton, A. A., & Dixon, S. J. (2018). Microplastics: An introduction to environmental transport processes. WIREs Water, 5(2), e1268. https://doi.org/10.1002/wat2.1268

Jung, U., & Choi, S. S. (2022). Classification and characterization of tire-road wear particles in road dust by density. Polymers, 14(5), 1005. https://doi.org/10.3390/polym14051005

Kayhanian, M., McKenzie, E. R., Leatherbarrow, J. E., & Young, T. M. (2012). Characteristics of road sediment fractionated particles captured from paved surfaces, surface run-off and detention basins. Science of the Total Environment, 439, 172-186.

Kanhai, L. D. K., Gårdfeldt, K., Lyashevska, O., & Hassellöv, M. (2018). Microplastics in sub-surface waters of the Arctic Central Basin. Marine Pollution Bulletin, 130, 8-18. https://doi.org/10.1016/j.marpolbul.2018.03.011

Klein, S., Dimzon, I. K., Eubeler, J., & Knepper, T. P. (2018). Analysis, occurrence, and degradation of microplastics in the aqueous environment. In M. Wagner & S. Lambert (Eds.), Freshwater Microplastics: Emerging Environmental Contaminants? (pp. 51–67). Springer International Publishing. https://doi.org/10.1007/978-3-319-61615-5_3

Klöckner, P., Reemtsma, T., Eisentraut, P., Braun, U., Ruhl, A. S., & Wagner, S. (2019). Tire and road wear particles in road environment - Quantification and assessment of particle dynamics by Zn determination after density separation. Chemosphere, 222, 714-721.

Koelmans, A. A., Besseling, E., & Shim, W. J. (2015). Nanoplastics in the aquatic environment. Critical review. In: Marine anthropogenic litter. Springer, Berlin, pp. 325–340.

Kooi, M., Besseling, E., Kroeze, C., Van Wezel, A. P., & Koelmans, A. A. (2018). Modeling the fate and transport of plastic debris in freshwaters: Review and guidance. In M. Wagner & S. Lambert (Eds.), Freshwater Microplastics: Emerging Environmental Contaminants? (pp. 125–152). Springer International Publishing. https://doi.org/10.1007/978-3-319-61615-5_7

Kreider, M. L., Panko, J. M., McAtee, B. L., Sweet, L. I., & Finley, B. L. (2010). Physical and chemical characterization of tire-related particles: Comparison of particles generated using different methodologies. Science of the Total Environment, 408(3), 652-659.

Kukulka, T., Proskurowski, G., Morét-Ferguson, S., Meyer, D. W., & Law, K. L. (2012). The effect of wind mixing on the vertical distribution of buoyant plastic debris. Geophysical Research Letters, 39(7), L07601. https://doi.org/10.1029/2012GL051116

Kwak, J. H., Kim, H., Lee, J., & Lee, S. (2013). Characterization of non-exhaust coarse and fine particles from on-road driving and laboratory measurements. Science of the Total Environment, 458–460, 273-282.

Lambert, S., & Wagner, M. (2016). Characterisation of nanoplastics during the degradation of polystyrene. Chemosphere, 145, 265-268. https://doi.org/10.1016/j.chemosphere.2015.11.078

Lavin, P. (2003). Estimating and specifying asphalt pavements. In: Asphalt pavements: A practical guide to design, production and maintenance for engineers and architects. Spon Press: London, England. p. 403.

Lechthaler, S., Waldschläger, K., Stauch, G., & Schüttrumpf, H. (2020). The way of macroplastic through the environment. Environments, 7, 73 (2020).

Li, H., Harvey, J. T., Asselanis, J., Zhou, J., Guada, I. M., Kannekanti, V. N., & Wu, R. (2016). Results from visual inspection and laboratory testing for ASR in existing concrete cores from bridges and pavements in California. California Department of Transportation Research Report: UCPRC-RR-2015-07.

Magnin, A., Pollet, E., Phalip, V., & Avérous, L. (2020). Evaluation of biological degradation of polyurethanes. Biotechnology Advances, 39, 107457. https://doi.org/10.1016/j.biotechadv.2019.107457

Mennekes, D., & Nowack, B. (2023). Predicting microplastic masses in river networks with high spatial resolution at country level. Nature Water, 1, 523-533. https://doi.org/10.1038/s44221-023-00090-9

Min, K., Cuiffi, J. D., & Mathers, R. T. (2020). Ranking environmental degradation trends of plastic marine debris based on physical properties and molecular structure. Nature Communications, 11(1), 727. https://doi.org/10.1038/s41467-020-14538-z

Mishra, S., Swain, S., Sahoo, M., Mishra, S., & Das, A. P. (2021). Microbial colonization and degradation of microplastics in aquatic ecosystems: A review. Geomicrobiology Journal, 39(3–5), 259–269. https://doi.org/10.1080/01490451.2021.1983670

Morales-Caselles, C., Viejo, J., Marti, E., González Fernández, D., Pragnell-Raasch, H., González-Gordillo, J., Montero, E., Munoz Arroyo, G., Hanke, G., Salvo, V.-S., Basurko, O., Mallos, N., Lebreton, L., Echevarría, F., van Emmerik, T., Duarte, C., Gálvez, J., Galgani, F., García, C., & Cózar, A. (2021). An inshore-offshore sorting system revealed from global classification of ocean litter. Nature Sustainability, 4. https://doi.org/10.1038/s41893-021-00720-8

Nizzetto, L., Bussi, G., Futter, M. N., Butterfield, D., & Whitehead, P. G. (2016). A theoretical assessment of microplastic transport in river catchments and their retention by soils and river sediments. Environmental Science: Processes & Impacts, 18(1050–1059), 8.

Oldenkamp, R. et al. (2013). Spatially explicit prioritization of human antibiotics and antineoplastics in Europe. Environment International, 51(0), 13-26.

Patrizia Pfohl, Marion Wagner, Lars Meyer, Prado Domercq, Antonia Praetorius, Thorsten Hüffer, Thilo Hofmann, and Wendel Wohlleben. Environmental Degradation of Microplastics: How to Measure Fragmentation Rates to Secondary Micro- and Nanoplastic Fragments and Dissociation into Dissolved Organics. Environmental Science & Technology 2022 56 (16), 11323-11334

Reineccius, J., Schönke, M., & Waniek, J. J. (2023). Abiotic long-term simulation of microplastic weathering pathways under different aqueous conditions. Environmental Science & Technology, 57(2), 963-975. https://doi.org/10.1021/acs.est.2c05746

Rhodes, E. P., Ren, Z. Y., & Mays, D. C. (2012). Zinc leaching from tire crumb rubber. Environmental Science & Technology, 46, 12856-12863

Rowley, K., Cucknell, A., Smith, B., Clark, P., & Morritt, D. (2020). London's river of plastic: High levels of microplastics in the Thames water column. Science of the Total Environment, 740, 140018. https://doi.org/10.1016/j.scitotenv.2020.140018

Rødland, E. S., Gustafsson, M., Jaramillo-Vogel, D., Järlskog, I., Müller, K., Rauert, C., Rausch, J., & Wagner, S. (2023). Analytical challenges and possibilities for the quantification of tire-road wear particles. TrAC Trends in Analytical Chemistry, 165, 0165-9936. https://doi.org/10.1016/j.trac.2023.117121

Sarkar, D. J., Sarkar, S., Das, B., Sahoo, B., Das, A., Nag, S., Manna, R., Behera, B., & Samanta, S. (2021). Occurrence, fate and removal of microplastics as heavy metal vector in natural wastewater treatment wetland system. Water Research, 192, 116853. https://doi.org/10.1016/j.watres.2021.116853

Sansalone, J., & Tribouillard, T. (1999). Variation in characteristics of abraded roadway particles as a function of particle size: Implications for water quality and drainage. Transportation Research Record, 1690, 153-163.

Shah, A. A., Hasan, F., Hameed, A., & Ahmed, S. (2008). Biological degradation of plastics: A comprehensive review. Biotechnology Advances, 26(3), 246-265. https://doi.org/10.1016/j.biotechadv.2007.12.005

Van Melkebeke, M., Janssen, C., & De Meester, S. (2020). Characteristics and sinking behavior of typical microplastics including the potential effect of biofouling: Implications for remediation. Environmental Science & Technology, 54(14), 8668-8680.

Victor Onink, Mikael L. A. Kaandorp, Erik van Sebille, and Charlotte Laufkötter. Influence of Particle Size and Fragmentation on Large-Scale Microplastic Transport in the Mediterranean Sea. Environmental Science & Technology 2022 56 (22), 15528-15540 DOI: 10.1021/acs.est.2c03363

Von Smoluchowski, M. (1917). Versuch einer mathematischen Theorie der Koagulationskinetik kolloider Lösungen. Zeitschrift fuer Phys. Chemie, 92, 129-168

Wagner et al., 2018. S. Wagner, T. Hüffer, P. Klöckner, M. Wehrhahn, T. Hofmann, & Reemtsma, T. Tire wear particles in the aquatic environment - A review on generation, analysis, occurrence, fate and effects. Water Research, 139, 83-100

Waldschläger, K., Lechthaler, S., Stauch, G., & Schüttrumpf, H. (2020). The way of microplastic through the environment – Application of the source-pathway-receptor model (review). Science of The Total Environment, 713, 136584. https://doi.org/10.1016/j.scitotenv.2020.136584

Wallis, S. (2007). "The numerical solution of the advection-dispersion equation: A review of some basic principles". Acta Geophysica, 5.1, 85–94.

Wang, Q., Zhang, Q., Wu, Y., & Wang, X. C. (2017). Physicochemical conditions and properties of particles in urban runoff and rivers: Implications for runoff pollution. Chemosphere, 173, 318-325. https://doi.org/10.1016/j.chemosphere.2017.01.066

Wang, T., Wang, L., Chen, Q., Kalogerakis, N., Ji, R., & Ma, Y. (2020). Interactions between microplastics and organic pollutants: Effects on toxicity, bioaccumulation, degradation, and transport. Science of The Total Environment, 748, 142427. https://doi.org/10.1016/j.scitotenv.2020.142427

Yuan, J., Ma, J., Sun, Y., Zhou, T., Zhao, Y., & Yu, F. (2020). Microbial degradation and other environmental aspects of microplastics/plastics. Science of The Total Environment, 715, 136968. https://doi.org/10.1016/j.scitotenv.2020.136968

Zhang, K., Hamidian, A. H., Tubić, A., Zhang, Y., Fang, J. K. H., Wu, C., & Lam, P. K. S. (2021). Understanding plastic degradation and microplastic formation in the environment: A review. Environmental Pollution, 274, 116554. https://doi.org/10.1016/j.envpol.2021.116554

Zhang, K., Gong, W., Lv, J., et al. (2015). Accumulation of floating microplastics behind the Three Gorges Dam. Environmental Pollution, 204, 117-123.

Zhu, K., Jia, H., Sun, Y., Dai, Y., Zhang, C., Guo, X., ... & Zhu, L. (2020). Long-term phototransformation of microplastics under simulated sunlight irradiation in aquatic environments: Roles of reactive oxygen species. Water Research, 173, 115564. https://doi.org/10.1016/j.watres.2020.11.047

Zhu, K., Jia, H., Sun, Y., Dai, Y., Zhang, C., Guo, X., ... & Zhu, L. (2020). Long-term phototransformation of microplastics under simulated sunlight irradiation in aquatic environments: Roles of reactive oxygen species. Water Research, 173, 115564. https://doi.org/10.1016/j.watres.2020.11.047

## SUPPLEMENTARY MATERIALS

| *Parameter* | *Symbol* | *Value* | *Unit* |
|---|---|---|---|
| *River flow rate constant of box n* | $k_{flow,n}$ | $k_{flow,n} \cdot \frac{A_{w,n}}{Q_{w,n}}$ | $s^{-1}$ |
| *Settling velocity of MPs of size class i* | $v_{set,i}$ | *Eq.12* | *m/s* |
| *Settling velocity of SPMs of size class j* | $v_{set,j}$ | *Eq.21* | *m/s* |
| *Sedimentation rate constant of MPs of size class i* | $k_{sed,i}$ | $\frac{v_{set,i}}{H_{w,n}}$ | $s^{-1}$ |
| *Resuspension rate constant of MPs of size class i* | $k_{rusp,i}$ | $\frac{v_{rusp,i}}{H_{sed,n}}$ | $s^{-1}$ |
| *Heteroaggregation rate constant between MPs of size class i and SPM of size class j* | $k_{hetAgg,n}$ | *Eq.19* | $s^{-1}$ |
| *Rate constant of horizontal sediment transfer of box n* | $k_{sedtransfer,n}$ | *Eq.22* | $s^{-1}$ |

*Table S1. Rate constants of processes in the model*